

What is the nature of GW230529? An exploration of the gravitational lensing hypothesis

Justin Janquart^{1,2,3,4*}, David Keitel^{5,6†}, Rico K. L. Lo^{7‡}, Juno C. L. Chan⁷, Jose María Ezquiaga⁷, Otto A. Hannuksela⁸, Alvin K. Y. Li^{9,8,10}, Anupreeta More^{11,12}, Hemantakumar Phurailatpam⁸, Neha Singh⁵, Laura E. Uronen⁸, Mick Wright¹³, Naresh Adhikari¹⁴, Sylvia Biscoveanu¹⁵, Tomasz Bulik¹⁶, Amanda M. Farah¹⁷, Anna Heffernan⁵, Prathamesh Joshi^{18,19}, Vincent Juste²⁰, Atul Kedia²¹, Shania A. Nichols²², Geraint Pratten²³, C. Rawcliffe²⁴, Soumen Roy^{4,3,1,2}, Elise M. Sänger²⁵, Hui Tong^{26,27}, M. Trevor²⁸, Luka Vujeva⁷, Michael Zevin^{29,15}

¹Center for Cosmology, Particle Physics and Phenomenology - CP3, Université Catholique de Louvain, Louvain-La-Neuve, B-1348, Belgium

²Royal Observatory of Belgium, Avenue Circulaire, 3, 1180 Uccle, Belgium

³Department of Physics, Utrecht University, Princetonplein 1, 3584 CC Utrecht, The Netherlands

⁴Nikhef, Science Park 105, 1098 XG Amsterdam, The Netherlands

⁵Departament de Física, Universitat de les Illes Balears, IAC3-IEEC, E-07122 Palma, Spain

⁶University of Portsmouth, Institute of Cosmology and Gravitation, Portsmouth PO1 3FX, United Kingdom

⁷Niels Bohr International Academy, Niels Bohr Institute, Blegdamsvej 17, DK-2100 Copenhagen, Denmark

⁸Department of Physics, The Chinese University of Hong Kong, Shatin, New Territories, Hong Kong

⁹LIGO Laboratory, California Institute of Technology, Pasadena, CA 91125, USA

¹⁰RESCEU, The University of Tokyo, Tokyo, 113-0033, Japan

¹¹The Inter-University Centre for Astronomy and Astrophysics (IUCAA), Post Bag 4, Ganeshkhind, Pune 411007, India

¹²Kavli Institute for the Physics and Mathematics of the Universe (IPMU), 5-1-5 Kashiwanoha, Kashiwa-shi, Chiba 277-8583, Japan

¹³SUPA, School of Physics and Astronomy, University of Glasgow, Glasgow, Scotland

¹⁴Leonard E. Parker Center for Gravitation, Cosmology, and Astrophysics, University of Wisconsin–Milwaukee, Milwaukee, WI 53201, USA

¹⁵Center for Interdisciplinary Exploration and Research in Astrophysics (CIERA), Northwestern University, 2145 Sheridan Road, Evanston, IL, 60201, USA

¹⁶Astronomical Observatory, University of Warsaw, Aleje Ujazdowskie 4, 00478 Warsaw, Poland

¹⁷Department of Physics, University of Chicago, Chicago, IL 60637, USA

¹⁸Department of Physics, The Pennsylvania State University, University Park, PA 16802, USA

¹⁹Institute for Gravitation and the Cosmos, The Pennsylvania State University, University Park, PA 16802, USA

²⁰Service de Physique Théorique, CP225, Université Libre de Bruxelles, Boulevard du Triomphe, 1050 Bruxelles, Belgium

²¹Center for Computational Relativity and Gravitation, Rochester Institute of Technology, Rochester, New York 14623, USA

²²Louisiana State University, Baton Rouge, LA 70803, USA

²³School of Physics and Astronomy, University of Birmingham, Edgbaston, Birmingham, B15 2TT, United Kingdom

²⁴University of British Columbia, Vancouver, BC V6T 1Z4, Canada

²⁵Max Planck Institute for Gravitational Physics (Albert Einstein Institute), Am Mühlenberg 1, Potsdam, 14476, Germany

²⁶School of Physics and Astronomy, Monash University, VIC 3800, Australia

²⁷OzGrav: The ARC Centre of Excellence for Gravitational Wave Discovery, Clayton VIC 3800, Australia

²⁸University of Maryland, College Park, Maryland 20742, USA

²⁹The Adler Planetarium, 1300 South DuSable Lake Shore Drive, Chicago, 60605, IL, USA

ABSTRACT

On the 29th of May 2023, the LIGO–Virgo–KAGRA Collaboration observed a compact binary coalescence event consistent with a neutron star – black hole merger, though the heavier object of mass $2.5 – 4.5 M_{\odot}$ would fall into the purported lower mass gap. An alternative explanation for apparent observations of events in this mass range has been suggested as strongly gravitationally lensed binary neutron stars. In this scenario, magnification would lead to the source appearing closer and heavier than it really is. Here, we investigate the chances and possible consequences for the GW230529 event to be gravitationally lensed. We find this would require high magnifications and we obtain low rates for observing such an event, with a relative fraction of lensed versus unlensed observed events of 2×10^{-3} at most. When comparing the lensed and unlensed hypotheses accounting for the latest rates and population model, we find a 1/58 chance of lensing, disfavoring this option. Moreover, when the magnification is assumed to be strong enough to bring the mass of the heavier binary component below the standard limits on neutron star masses, we find high probability for the lighter object to have a sub-solar mass, making the binary even more exotic than a mass-gap neutron star–black hole system. Even when the secondary is not sub-solar, its tidal deformability would likely be measurable, which is not the case for GW230529. Finally, we do not find evidence for extra lensing signatures such as the arrival of additional lensed images, type-II image dephasing, or microlensing. Therefore, we conclude it is unlikely for GW230529 to be a strongly gravitationally lensed binary neutron star signal.

Key words: gravitational lensing – gravitational waves

1 INTRODUCTION

GW230529_181500 (for short GW230529, [LVK 2024a](#)) is a gravitational-wave (GW) signal from a compact binary coalescence (CBC) observed by the LIGO–Virgo–KAGRA collaboration (LVK) close to the start of its fourth observing run (O4a). Its component masses made GW230529 unusual, different from any events in the previous GWTC releases ([LVK 2023a](#)) from the Advanced LIGO ([Aasi et al. 2015](#)), Advanced Virgo ([Acernese et al. 2015](#)) and KAGRA ([Somiya 2012](#); [Aso et al. 2013](#); [Akutsu et al. 2020](#)) network. The standard interpretation is for the signal to originate from the merger of a neutron star with an object between 2.5 and $4.5 M_{\odot}$ ([LVK 2024a](#)). While confirming the exact nature of the heavier object is difficult with GW data alone, it seems most likely the source is not a binary neutron star (BNS) but rather a neutron star–black hole (NSBH) merger, with a light black hole in the so-called lower mass gap ([LVK 2024a](#)). Observations of low-mass X-ray binaries in the Galaxy do not show evidence of stellar mass black holes in this region of the mass spectrum ([Özel et al. 2010](#); [Farr et al. 2011](#)), and it is difficult to populate with standard stellar progenitor models. However, there is now growing evidence that this mass region is not completely empty ([LVK 2023b](#), [2024a](#)).

An alternative explanation for GW events observed with component masses in the lower mass gap is gravitational lensing of regular BNSs ([Bianconi et al. 2023](#); [Magare et al. 2023](#); [Canevarolo et al. 2024](#)). For magnified events, the inferred luminosity distance is lower than the true one, leading to an underestimation of the source redshift and hence overestimation of the source-frame masses. Therefore, the heavier component of a regular BNS could be mistaken for a mass-gap compact object. Without an electromagnetic counterpart, it is generally difficult to confirm the nature of the event, with or without lensing ([Bianconi et al. 2023](#)). An exception occurs when the tidal deformation of the binary leaves an imprint on the GW waveform, since the lensing hypothesis can be verified when the measured deformability is incompatible with the apparent masses for a realistic equation of state (EoS) ([Pang et al. 2020](#)). Other options

include finding multiple lensed copies (images) of GWs from the same source (e.g., [Haris et al. 2018](#)), overlapping signals in the high-magnification limit ([Lo et al. 2024](#)), and frequency-dependent lensing effects on the waveform ([Takahashi & Nakamura 2003](#)), their image type ([Dai & Venumadhav 2017](#); [Ezquiaga et al. 2021](#)), or finding additional microlensing features (e.g., [Mishra et al. 2021](#)). Due to the limited current BNS detection range, lensing rates for such events are however low, as the lensing optical depth is small at low redshifts. This is why GW lensing searches have so far mainly focused on binary black holes (BBHs), which can be detected from further away ([Hannuksela et al. 2019](#); [LVC 2021](#); [LVK 2024b](#); [Janquart et al. 2023b](#))

In this work, we investigate the possibility of GW230529 being a lensed BNS appearing as a NSBH merger when analysed under the unlensed hypothesis. This work is structured as follows. In Section 2, we describe GW230529 in more detail, including some discussions on the implications of the event if it is not lensed. In Section 3, we describe the basics of gravitational lensing of GWs, and explain how it can lead to biased estimates of the source parameters. Then, in Section 4, we discuss the detection rates of lensed BNS signals with O4a sensitivity and the expected characteristics of such events. We then consider in Section 5 whether a lensed GW230529 would be more consistent with population models, and compute a Bayes factor for this. In Section 6, we check explicitly what the source-frame parameters of the event could be if it was lensed, finding the source likely would be some other type of exotic binary system, including a sub-solar mass object. Here, we also look at whether we would expect to be able to measure the tidal deformabilities for lensed signals matching GW230529. In Section 7, we do extra checks to search for lensing features including multiple images, negative image parity, and microlensing effects. We summarize our findings and discuss the implications in Section 8.

2 A BRIEF DESCRIPTION OF GW230529

GW230529 ([LVK 2024a](#)) was observed on the 29th of May 2023, at 18:15:00.7 UTC, by the LIGO Livingston detector. LIGO Hanford was out of observing mode and Virgo was undergoing upgrades. KAGRA was in observing mode, but its sensitivity was too low to

* justin.janquart@uclouvain.be

† david.keitel@ligo.org

‡ kalok.lo@nbi.ku.dk

impact the analysis of the event. The event was observed by three matched-filter pipelines: GSTLAL (Messick et al. 2017; Sachdev et al. 2019; Hanna et al. 2020; Cannon et al. 2021; Ewing et al. 2023; Tsukada et al. 2023), PyCBC (Allen 2005; Allen et al. 2012; Dal Canton et al. 2021; Usman et al. 2016; Nitz et al. 2017; Davies et al. 2020), and MBTA (Adams et al. 2016; Aubin et al. 2021), with similar signal-to-noise ratio (SNR) of about 11.4 in all of them.

Bayesian parameter estimation under standard LVK priors¹ gave 90% credible intervals of 201_{-96}^{+102} Mpc for the luminosity distance D_L and source-frame component masses of $3.6_{-1.2}^{+0.8} M_\odot$ and $1.4_{-0.2}^{+0.6} M_\odot$ for the heavier (primary) and lighter (secondary) component, respectively. Therefore, the primary is likely in the mass-gap region, taken as $3-5 M_\odot$ (LVK 2024a; Özel et al. 2010; Farr et al. 2011), and it would be of high interest to know whether it is a neutron star or a black hole.

Finding an electromagnetic counterpart could help answer this question. However, as a single-detector observation, sky localization was poor, making electromagnetic follow-ups difficult. Chandra et al. (2024) have reported that a BNS kilonova from the event could have been detectable with a telescope like the future Rubin Observatory (Ivezic et al. 2019), but no counterparts have been reported from telescopes available at the time, with constraints reported in several wavelengths (Ronchini et al. 2024; Ahumada et al. 2024).

The most direct GW-only test of the nature of the component objects would be signatures of tidal deformability in the GW waveform. The LVK analysis with a BNS waveform (IMRPhenomPv2_NRTidalv2, Dietrich et al. 2019) returned a posterior on the tidal deformability of the primary that peaks at zero, compatible with a black hole. Even though it falls off clearly towards higher values, it is too broad to confidently exclude the possibility of a neutron star. For the secondary, the posterior on the tidal deformability is uninformative, whether the event is analyzed with a BNS waveform or one for NSBHs (IMRPhenomNSBH and SEOBNRv4_ROM_NRTidalv2_NSBH, Thompson et al. 2020; Matas et al. 2020). Therefore, one cannot tell whether the event is an NSBH or a BNS this way.

A more indirect approach is to check the spins of the components, since neutron stars are expected to have spin amplitudes below 0.05 (O’Shaughnessy et al. 2008). However, spins are partially degenerate with masses (Cutler & Flanagan 1994), and difficult to measure individually for the two components (Vitale et al. 2017; Shaik et al. 2020). This made it challenging to tell whether the primary has a high spin or not.

Further tests were done to evaluate the probability of the primary being a neutron star under different hypotheses. To do so, LVK (2024a) looked at the probability of its mass being below the maximum allowed for a neutron star, while marginalizing over the measured masses and spins, and different EoSs (LVK 2023b; Essick & Landry 2020). Allowing for large spins in the prior ($\chi_1, \chi_2 \leq 0.99$)², a $2.9_{-0.4}^{+0.4}\%$ probability was found for the primary to be a neutron star. Restricting the spins to low values, i.e. $\chi_1, \chi_2 \leq 0.05$, this probability dropped below 0.1%. Finally, accounting for a POWER LAW + DIP + BREAK population prior (Fishbach et al. 2020; Farah et al. 2022; LVK 2023b), a probability of $8.8_{-2.8}^{+2.8}\%$ was found, taking into account that this prior leads to lower posterior mass estimates for the primary. On the contrary, the probability of the secondary to be a neutron star is higher than 95% in all cases. Similarly, Koehn et al. (2024) obtained $\gtrsim 84\%$ probability for the primary to be a black hole using observa-

¹ Using a BBH waveform with low-mass priors, and combining the results of different waveforms to mitigate potential systematics (LVK 2024a).

² χ_i is the amplitude of the dimensionless spin vector of component i .

tionally constrained EoSs. The impact of population-informed spin priors was further investigated by Chattopadhyay et al. (2024), finding consistent but potentially tighter mass estimates. In summary, the preferred scenario under standard astrophysical assumptions is that of an NSBH merger, with a black hole in the mass-gap region.

Finally, assuming GW230529 came from an NSBH, there are also consequences for the mass distribution of black holes in such mergers, with a decrease in the lowest expected mass of black holes, and an increased chance of having a black hole sub-population in the mass gap (LVK 2024a). This also means that one needs to revisit the formation scenarios for such mergers to find compelling explanations for their observation. Some such studies have already been conducted, e.g. by Zhu et al. (2024); Chandra et al. (2024); Ye et al. (2024). More exotic scenarios have also been considered, such as primordial black holes (Huang et al. 2024). The event has also already been used to perform tests of general relativity (Gao et al. 2024; Sänger et al. 2024; Julié et al. 2024), where constraints are particularly tight if the primary can be assumed to be a black hole.

3 GRAVITATIONAL LENSING OF GRAVITATIONAL WAVES

When a GW passes close to a massive object when travelling from the source to an observer, it can be gravitationally lensed (Ohanian 1974; Deguchi & Watson 1986; Wang et al. 1996; Nakamura 1998; Takahashi & Nakamura 2003), modifying the observed waveform. The effect depends on the mass of the deflector and the lens-source geometry. For the heaviest objects—galaxies or galaxy clusters—and best-aligned cases, we have strong lensing (Dai & Venumadhav 2017; Haris et al. 2018; Ezquiaga et al. 2021; Liu et al. 2021; Lo & Magana Hernandez 2023; Janquart et al. 2021a, 2023a). In this case, the GW signal is split into multiple potentially detectable copies—referred to as “images”—originating from the same sky location (within GW detector accuracy) but magnified, with a resolvable time delay, and with an overall phase shift (Dai & Venumadhav 2017; Ezquiaga et al. 2021). The regimes for lower-mass lenses or less alignment are often called millilensing, where images with short time delays overlap in the detector band (Liu et al. 2023), and microlensing, where the waveform deformations due to lensing become frequency-dependent instead (Takahashi & Nakamura 2003; Wright & Hendry 2021).

While the probability of detecting such phenomena is currently relatively low, it increases as detector sensitivity improves and as more detectors are added to the global network (Ng et al. 2018; Li et al. 2018; Oguri 2018; Wierda et al. 2021; Xu et al. 2022). Searches for lensing signatures in the LVK data, focusing on BBH signals, have not yet provided compelling evidence for lensing (Hannuksela et al. 2019; Dai et al. 2020; LVC 2021; LVK 2024b; Janquart et al. 2023b).

Multiple images of CBC events can be searched for with a variety of methods (Haris et al. 2018; McIsaac et al. 2020; Li et al. 2023b; Liu et al. 2021; Janquart et al. 2021a; Lo & Magana Hernandez 2023; Goyal et al. 2021; Janquart et al. 2023a; Ezquiaga et al. 2023; Li et al. 2023a; Magare et al. 2024). Effects that modify the waveforms, including microlensing, millilensing, and type-II strongly lensed images, can also be detected from a single signal directly, provided the effect is large enough (Wright & Hendry 2021; Janquart et al. 2021b; Wang et al. 2021; Vijaykumar et al. 2023; Liu et al. 2023). In the particular case of a lensed BNS signal, it could also be identified as lensed by inspecting the measured tidal deformability, as the source

masses and tidal parameters inferred without accounting for lensing would become incompatible for realistic EoSs (Pang et al. 2020).

3.1 Strong Lensing

Most of the discussion in this paper concerns the strong lensing scenario, hence we give here some more details on this regime. In the frequency domain, the GW waveform of the i^{th} lensed image (h_L^i) is related to that of the original unlensed signal (h_{NL}) as

$$h_L^i(f; \boldsymbol{\theta}, \phi_i) = \sqrt{\mu_i} h_{\text{NL}}(f; \boldsymbol{\theta}) e^{(2i\pi f \Delta t_i - i\pi n_i \text{sign}(f))}, \quad (1)$$

where $\boldsymbol{\theta}$ are the usual binary parameters, and $\phi_i = \{\mu_i, \Delta t_i, n_i\}$ are the lensing parameters for image i , with the magnification μ_i , the time delay Δt_i , and the Morse factor n_i (Dai & Venumadhav 2017; Ezquiaga et al. 2021). The latter can only take three values: $n_i = 0, 0.5, 1$, corresponding to so-called image types I, II, and III, respectively (Ezquiaga et al. 2021). Only type-II images can potentially leave a detectable imprint on lensed GW signals (Ezquiaga et al. 2021; Wang et al. 2021; Janquart et al. 2021b; Vijaykumar et al. 2023).

From Eq. (1), we see that some lensing parameters are degenerate with the source parameters. In particular, the amplitude of the unlensed signal is proportional to $1/D_L$, which is a simple prefactor like the magnification. Additionally, the time of arrival of a lensed signal is $t_c + \Delta t_i$, combining the usual time of coalescence, t_c , and the lensing time delay. So, both the magnification and the time delay are degenerate with the luminosity distance and the time of coalescence, respectively. When estimating these parameters under the unlensed hypothesis, we actually measure *effective* parameters

$$D_L^{\text{eff}} = \frac{D_L}{\sqrt{\mu_i}}, \quad (2)$$

$$t_c^{\text{eff}} = t_c + \Delta t_i. \quad (3)$$

With a single GW image and no extra information (either external or from a distortion of the waveform), it is not possible to disentangle the lensing effect from the true distance to the source and its intrinsic properties in all generality. However, when several images are observed, it is possible to do *lens reconstruction* to find the parameters of the lens–source system and infer the time delay and magnification of each image (Hannuksela et al. 2020; Wempe et al. 2022; Wright et al. 2023; Seo et al. 2023; Poon et al. 2024).

If not accounted for, lensing can also lead to biased source parameter estimation. There is a general redshift–mass degeneracy in CBC signals because we observe the redshifted signal and have a direct GW measurement of the luminosity distance but not of the redshift. Therefore, the observed detector-frame mass, m^{det} , for a binary component is

$$m^{\text{det}} = (1 + z_s) m^{\text{src}}, \quad (4)$$

with z_s the redshift of the source and m^{src} the source-frame mass. The inferred source-frame mass is

$$m_{\text{inf}}^{\text{src}} = \frac{m^{\text{det}}_{\text{measured}}}{1 + z_s(D_{L,\text{measured}})}, \quad (5)$$

where $m^{\text{det}}_{\text{measured}}$ is the measured detector-frame mass, and $z_s(D_{L,\text{measured}})$ is the redshift inferred from the measured luminosity distance and a cosmological model.

Therefore, if the luminosity distance is biased by lensing, the inferred source-frame masses will also be biased, and we will infer a higher (lower) source frame mass than the real one for a magnified (demagnified) signal. This also means that exceptionally high-mass BBH events could potentially be explained through lensing (LVC

2021; Diego et al. 2021), though no compelling evidence has been found for this so far (LVC 2021). Similarly, some BNS events could be identified as NSBH events with a mass-gap component (Bianconi et al. 2023; Magare et al. 2023; Canevarolo et al. 2024).

3.2 Lensed Binary Neutron Star Mergers

When an observed CBC contains a neutron star, the GW signal also carries imprints of matter effects. For example, BNSs have complicated post-merger behaviors (Bauswein et al. 2012, 2014; Bernuzzi et al. 2015; Tsang et al. 2019) while the inspiral already is affected by the deformation of the neutron stars due to tidal forces (Hinderer et al. 2010; Damour & Nagar 2009) and due to their own rotation (Laarakkers & Poisson 1999; Poisson 1998; Harry & Hinderer 2018). This tidal deformation can be used to probe the internal structure and EoS (Agathos et al. 2015; Samajdar & Dietrich 2019; LVC 2018) of neutron stars. The deformation of a neutron star due to the gravitational field of its companion is described by the tidal deformability (Flanagan & Hinderer 2008; Hinderer et al. 2010)

$$\Lambda = \frac{2}{3} k_2 \left(\frac{c^2 R}{G m} \right)^5, \quad (6)$$

where k_2 is the Love number, R is the neutron star radius, and m is its mass. To calculate the value of this parameter for a given mass, one needs to solve the Tolman–Oppenheimer–Volkoff (TOV) equation assuming an EoS (Hinderer et al. 2010).

In a BNS GW signal, the leading-order tidal effects are encoded in

$$\tilde{\Lambda} = \frac{16}{13} \sum_{i=1,2} \Lambda_i \frac{m_i^4}{M^4} \left(12 - 11 \frac{m_i}{M} \right), \quad (7)$$

where $M = m_1 + m_2$ is the total mass. So, the best measured effect is a combination of the masses and tidal deformabilities. The individual tidal deformabilities are dimensionless and not affected by cosmological redshift. In $\tilde{\Lambda}$, the redshift dependency of the masses cancels out in the ratios, so it is not changed by redshift either when converting between the detector and source frames.

To detect lensed BNSs, one can leverage this fact that the inferred masses are biased by the lensing effect, while the tidal deformabilities are not, and both quantities are related (Pang et al. 2020). When an event with measurable tidal deformability is unlensed, then the deformability calculated from the inferred masses (for a given EoS) should coincide with the measurement directly from the GW data. On the other hand, if the event is lensed, the inferred masses are biased towards higher values due to the image magnification, leading to lower calculated values of the tidal deformability. Under sufficiently strong magnification, there would be a noticeable mismatch between the calculated and measured values, showing the event is lensed.

Moreover, should one have an accurate measurement of the tidal deformability, one can correct the recovered parameters for the lensing effect by finding a magnification such that the measured and calculated tidal deformabilities match. Alternatively, one can leverage this effect to account for lensing and compare the obtained event characteristics under the lens hypothesis with those expected from lensed BNS population simulations. This can be used to assess whether a given event is a lensed BNS candidate. For this to work, we however need to be able to measure the tidal deformability and have a sufficient lensing effect on the parameters. The former requires a loud signal, and the latter requires relatively high magnifications (Pang et al. 2020).

4 RATES AND PROPERTIES OF LENSED BNS EVENTS

In this section, we first discuss general predictions for the rates of lensed BNSs, and then focus on the case of high magnifications, as would likely be needed to explain GW230529 as a lensed BNS event.

4.1 Rates from different population models

Based on our expectations for source (CBC) and lens populations, we can calculate the detection rate for strongly lensed CBCs (Ng et al. 2018; Li et al. 2018; Oguri 2018; Xu et al. 2022; Mukherjee et al. 2021; Wierda et al. 2021; Magare et al. 2023). In particular, we need to assume some mass and redshift distributions for the CBCs, a mass profile model and redshift distribution for the lenses, and a strong lensing optical depth. Calculating the rate of lensed events requires simulating a large number of sources and lenses and then evaluating the rate of detectable lensed events (Phurailatpam et al. 2024) as

$$\mathcal{R} = \mathcal{N}^L \langle P(\text{obs}|z_s, \theta, \theta_L, z_l, \beta, \text{SL}) \rangle_{z_s \in P(z_s|\text{SL}), z_l \in P(z_l|z_s, \text{SL}), \theta \in P(\theta, \theta_L \in P(\theta_L|z_l, z_s, \text{SL}), \beta \in P(\beta|z_s, z_l, \theta_L, \text{SL}))} \quad (8)$$

where $P(\text{obs}|\dots, \text{SL})$ is the probability of a strongly lensed (“SL”) event being observed and $\langle \dots \rangle$ indicates integrating it over the priors of all the listed dependencies. Also, \mathcal{N}^L is the normalising factor

$$\mathcal{N}^L = \int_{z_{\min}}^{z_{\max}} R(z_s) P(\text{SL}|z_s) \frac{1}{(1+z_s)} \frac{dV_c}{dz_s} dz_s, \quad (9)$$

z_s is the source redshift, z_l is the redshift of the galaxy lens, θ defines the source parameters, θ_L defines the lens parameters, and β denotes the source position. $R(z_s)$ is the merger rate density distribution regardless of whether the source is detectable or not, $P(\text{SL}|z_s)$ is the probability of strong lensing for a source at redshift z_s , and dV_c/dz_s is the differential co-moving volume at redshift z_s .

We also note that this $P(\text{obs}|\dots, \text{SL})$ depends on the SNR of each event and on a threshold SNR (SNR_{cut}). The latter is used as a proxy for detectability, and a value of 8 is a common approximation, though see Essick (2023) for a more subtle discussion.

To have a sense of the dependence of the expected rates on the input models, we look at three different source distribution models:

- a uniform mass distribution between 1 and $3 M_\odot$ (a rather conservative upper limit for neutron star masses) with the merger-rate density from Wierda et al. (2021),
- a bimodal Gaussian mass model from Wysocki et al. (2019) with the merger-rate density from Wierda et al. (2021),
- and the mass model and merger-rate density from the population synthesis run M43.A of Belczynski et al. (2020)³.

For the simulations with all three of these populations, we present results assuming singular isothermal ellipsoid (SIE) lenses (Koopmans et al. 2009). We also performed comparisons with singular isothermal spheres (SIS, Witt 1990), finding broadly consistent results.

Differences in these three setups can lead to different results on rates both directly and through causing different selection biases. For example, models with lower source masses may lead to higher magnifications because the events needs a stronger boost from lensing to be detectable for a given distance.

For all models, we perform simulations and calculate the rates

³ We also investigated multiple other models from Belczynski et al. (2020), of which M43.A is the one with the highest local merger-rate density among those compatible with the latest LVK observed rates (LVK 2023b). (See Table 3 in Belczynski et al. (2020) for details.)

| Population | Unlensed rate [yr ⁻¹] | Lensed rate [yr ⁻¹] | Relative rate |
|------------------|--------------------------------------|------------------------------------|----------------------|
| Uniform mass | 7.1×10^{-1} | 1.5×10^{-3} | 2.1×10^{-3} |
| Bimodal Gaussian | 3.9×10^{-1} | 7.0×10^{-4} | 1.8×10^{-3} |
| M43.A | 1.6 | 2.0×10^{-4} | 1.2×10^{-4} |

Table 1. Unlensed detected event rates, lensed detected event rates, and relative lensed rates from our various LER-based simulations with different mass distributions and merger-rate functions.

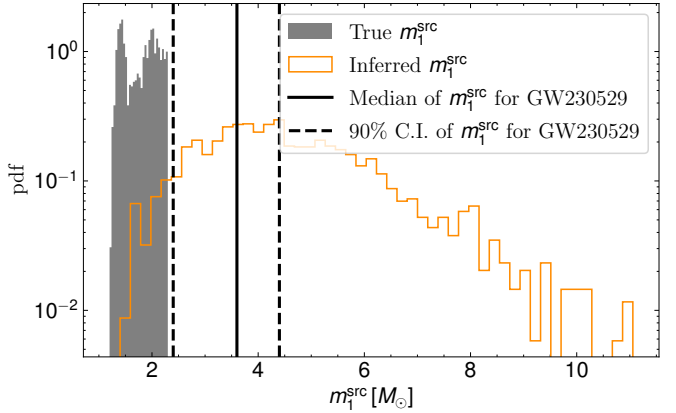


Figure 1. Example of how BNSs can appear as NSBHs if they are lensed but analyzed under the unlensed hypothesis. Here we show a bimodal mass distribution of true source-frame primary component masses. We compare it with the distribution one would infer from observations of lensed events from this population without accounting for lensing. Neglecting the lensing effect can lead to overestimated masses, pushing neutron stars into the $3-5 M_\odot$ mass gap. Overlaid are the median and 90% credible interval (C.I.) bounds for GW230529 (LVK 2024a).

using the LER package (Phurailatpam et al. 2024). We assume a single LIGO-Livingston detector with the noise power spectral density (PSD) from the GW230529 LVK data release (LVK 2024c). We require only one of the lensed images to pass the SNR threshold of 8, since only one event with properties similar to those for GW230529 was observed. (See Section 7.1 for a check on this assumption.)

While some variations (of a factor of a few) are seen in the relative lensing rate from one model to another, our calculations all agree that the relative detection rate of lensed versus unlensed events is smaller than $\approx 2 \times 10^{-3}$, see Table 1. Hence, from prior expectations alone, it is unlikely for an event like GW230529 to be lensed.

From the population simulations that go into these rate calculations, we can also extract information about expected properties of the lensed population. This is shown in Fig. 1, generated from the simulation with model (ii). As has already been shown in other works (Bianconi et al. 2023; Magare et al. 2023; Canevarolo et al. 2024), this demonstrates that for many lensed BNSs, the heavier component object appears to fall into the mass gap if source masses are inferred without accounting for lensing. Nevertheless, the relative rates found for this and the other models show that it is very unlikely to observe such a lensed BNS event at O4a sensitivity.

4.2 Probability of high-magnification BNS events

The LER rate calculations work by simulating a large number of lensed and unlensed events, then testing their detectability. We can thus also obtain the expected distribution of the lensing parameters

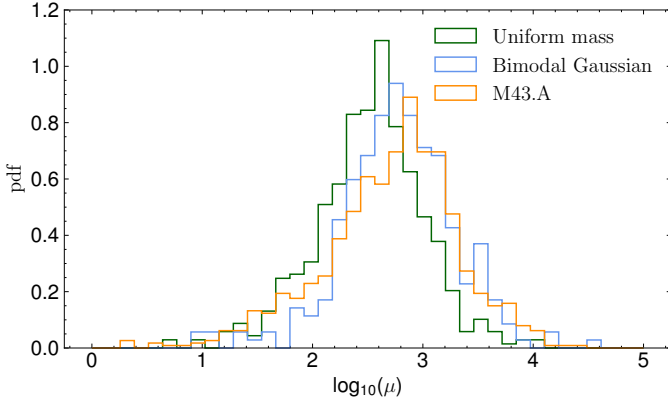


Figure 2. Histograms of the expected magnifications for detectable lensed BNS signals for the three simulations in our analysis. All three population models, representing different source mass models and merger-rate density functions, predict similar distributions.

| Magnification | Uniform mass | Bimodal Gaussian | M43.A |
|---------------|--------------|------------------|-------|
| $\geq 10^2$ | 86.6% | 93.8% | 87.2% |
| $\geq 10^3$ | 14.1% | 31.4% | 31.9% |
| $\geq 10^4$ | 0.4% | 1.1% | 0.9% |

Table 2. Probability to observe a magnification larger than a given threshold value in a detectable lensed BNS event, according to our various LER-based simulations with different mass distributions and merger-rate functions. In all cases, the percentage of detectable events with magnification $\geq 10^3$ is quite substantial, while magnifications $\geq 10^4$ are rare.

for detectable lensed events. In particular, we can see how often detectable lensed BNSs would be magnified enough that they can be confused with mass-gap events. For simplicity, here we limit source redshifts to $z_{\max} = 2$. This is sufficient because the detection horizon for unlensed BNSs is low, so that detectable lensed events from even higher redshifts would require even higher magnifications than what is needed for GW230529 to be shifted into the BNS range. (This will be demonstrated explicitly in Section 6.1.)

The magnification distributions obtained for the three models are represented in Fig 2. We see that different mass and merger-rate density models predict similar distributions with high probabilities for magnification in the hundreds to thousands. Notably, these are the expected magnifications for detectable events only, *i.e.* they include selection effects. Across all lensed events (detectable or not), the standard result for the high-magnification limit is $p(\mu) \propto \mu^{-3}$ (Schneider et al. 1992). For example, this would make a magnification of $\mu = 10^3$ about 10^3 times less likely compared to $\mu = 10^2$, but due to events with higher magnification being detectable from further away and hence from a larger source population, this trend is significantly shallower in our results.

Based on these simulations, we can check how likely it is to observe highly magnified lensed BNSs appearing similar to the GW230529 observation. We have used the obtained samples to calculate the probability of observing magnifications at or above a certain threshold. The values are shown in Table 2. There is a slight difference depending on the source population considered, but the numbers are broadly in agreement: The bulk of the distributions is below $\geq 10^3$, but values $\geq 10^3$ are still quite plausible for all models, while values $\geq 10^4$ become rare in all simulations.

5 POPULATION CONSIDERATIONS FOR A LENSED GW230529

While it is believed that the evolution of single stars cannot readily produce compact objects between $3 - 5M_{\odot}$ (Özel et al. 2010; Farr et al. 2011), there are other channels that can partially populate the purported mass gap, such as a hierarchical merger of a BNS merger remnant with another neutron star. In fact, previous GW observations had already suggested that the mass gap might not be completely empty (LVK 2023b). LVK (2024a) provides a more detailed discussion on the possible formation mechanisms for GW230529.

With lensing, if the true source-frame mass of the primary component of GW230529 is less than what was inferred and away from the mass gap because of the magnification bias, then the binary system would indeed be more consistent with both prior GW observations and theoretical expectations. However, this alternative explanation would require lensing of the GW signal with a certain magnification, which is by itself rare. Here, we discuss this trade-off between population consistency and the probability of the lensing hypothesis, first qualitatively and then quantitatively by calculating a corresponding Bayes factor.

5.1 Qualitative considerations

To understand whether any gain in consistency with prior expectations by making the source lighter overall would be enough to outweigh the penalty of invoking a rare phenomenon such as lensing, we first need to consider a specific population model. Both for the lensed and unlensed scenarios, we assume that the overall CBC source population follows the POWER LAW + DIP + BREAK model (Fishbach et al. 2020; Farah et al. 2022), with its maximum-likelihood parameters as reported in LVK (2023b). The joint probability distribution of the component masses $p_{\text{pop}}(m_1^{\text{src}}, m_2^{\text{src}})$ from this population model is factorized as

$$p_{\text{pop}}(m_1^{\text{src}}, m_2^{\text{src}}) \propto p_{\text{pop}}(m_1^{\text{src}}) p_{\text{pop}}(m_2^{\text{src}}) \left(\frac{m_2^{\text{src}}}{m_1^{\text{src}}} \right)^{\beta} \Theta(m_1^{\text{src}} \geq m_2^{\text{src}}), \quad (10)$$

where $p_{\text{pop}}(m_{1,2}^{\text{src}})$ consists of two broken power laws (one for neutron stars and one for black holes, respectively) and a dip to model the relative scarcity between the two regions (the “mass gap”, though it is not completely empty in this model).

In Fig. 3, the probability distribution of the source-frame primary mass m_1^{src} from this model is shown. Even before any further calculation, we see that there is some support for the primary of GW230529 to be outside the mass gap *without* assuming any magnification, *i.e.* with the original inference from LVK (2024a). In the same figure, we also indicate what the inferred source-frame primary mass would be if the GW signal was magnified by some example magnification values of $\mu = 10, 100, 1000$. We see that with $\mu = 100$, more than half of the support moves outside of the mass gap, and accordingly, the probability density is increased by a factor of ≈ 3 . With $\mu = 1000$, most of the support would be in the standard neutron star region, outside the mass gap. However, as discussed in Section 4, higher magnifications are, in turn, less likely.

While a high magnification will push the primary to a lower mass and hence a higher consistency with the expected population, the mass of the secondary component, receiving the same correction factor, might be pushed towards the sub-solar region. This can be problematic because the secondary needs to be compact enough such that the two objects will not be in contact already before the GW emission due to their inspiral reaches the sensitive frequency band of the LVK detectors (~ 10 Hz). The neutron star minimum mass is

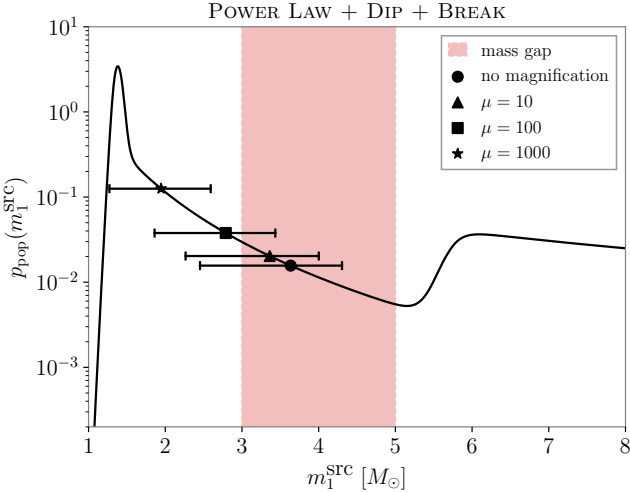


Figure 3. Probability distribution of the source-frame primary mass $p_{\text{pop}}(m_1^{\text{src}})$ of CBC sources as modeled by the POWER LAW + DIP + BREAK model. The shaded band indicates the purported mass gap from $3-5 M_{\odot}$. The median of the inferred m_1^{src} from LVK (2024a) without any magnification is shown as a dot, with the bars showing the 90% credible interval. In addition, the median and the uncertainty on the source-frame primary mass assuming a magnification of $\mu = 10$, $\mu = 100$ and $\mu = 1000$ are indicated by a triangle, a square and a star, respectively.

expected to be around $1 M_{\odot}$ (Suwa et al. 2018). While white dwarfs can be lighter, they do not have the necessary compactness and a neutron star–white dwarf binary will already be in contact at around ~ 0.2 Hz (Golomb et al. 2024). Therefore, for a sub-solar secondary, another exotic scenario such as a primordial black hole or other kinds of exotic compact objects will be needed.

We present joint probability distributions for both component masses in Fig. 4, both for the original results and under the same three example magnification values as before. We see that starting from $\mu \sim 10$, some of the support for the source-frame secondary mass m_2^{src} will be below $1 M_{\odot}$. For $\mu = 1000$, the primary component will be outside the mass gap, but most of the support for the secondary will be in the sub-solar region. This aspect will be discussed more in depth in Section 6.1.

5.2 Bayes factor calculation

We now consolidate all these considerations, both from the perspective of source population consistency and the relative probability of lensing with a certain magnification, into one single number—a Bayes factor $\mathcal{B}_{\text{NL}}^{\text{L}}$ between the lensed hypothesis \mathcal{H}_{L} and the not-lensed hypothesis \mathcal{H}_{NL} . Following Lo & Magana Hernandez (2023), it is defined as

$$\mathcal{B}_{\text{NL}}^{\text{L}} \equiv \frac{p(d_{\text{GW}}|\mathcal{H}_{\text{L}})}{p(d_{\text{GW}}|\mathcal{H}_{\text{NL}})}, \quad (11)$$

where $p(d_{\text{GW}}|\mathcal{H}_{\text{L}})$ and $p(d_{\text{GW}}|\mathcal{H}_{\text{NL}})$ are the marginal likelihoods for the observed data d_{GW} under each hypothesis. Considering only one possibly lensed signal, the marginal likelihood under \mathcal{H}_{L} is given by

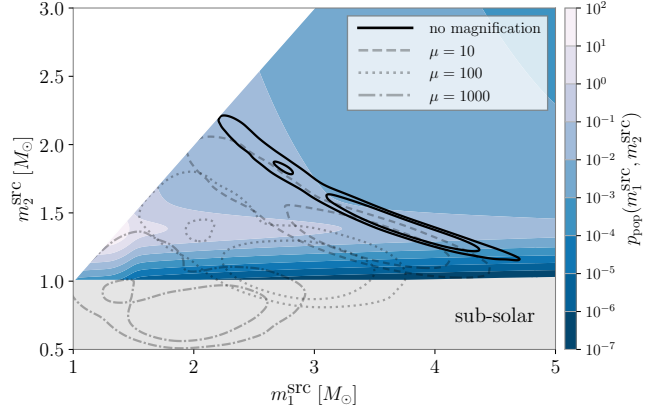


Figure 4. Joint probability distribution of the source-frame component masses $p_{\text{pop}}(m_1^{\text{src}}, m_2^{\text{src}})$ as modeled by the POWER LAW + DIP + BREAK model. As the magnification μ increases, the inferred source-frame component masses decrease (from the solid contours for $\mu = 1$ to the dash-dotted contours for $\mu = 1000$). In particular, when $\mu = 1000$, a large portion of the support for the secondary component mass lies in the sub-solar ($< 1 M_{\odot}$) region.

$$p(d_{\text{GW}}|\mathcal{H}_{\text{L}}) \propto \int dz_s p_{\text{pop}}(z_s|\mathcal{H}_{\text{L}}) \left[\sum_{n=0,1/2,1} \int dm_1^{\text{src}} dm_2^{\text{src}} d\mu \right. \\ \left. p(d_{\text{GW}}|m_{1,2}^{\text{det}} = (1 + z_s)m_{1,2}^{\text{src}}, D_{\text{L}} = \frac{D_{\text{L}}^{\text{src}}}{\sqrt{\mu}}, n) p_{\text{pop}}(m_1^{\text{src}}, m_2^{\text{src}}) p(\mu) \right], \quad (12)$$

where the term enclosed by the square brackets is the marginal likelihood $\mathcal{L}_{\mathcal{H}_{\text{L}}}(z_s)$ as a function of the source redshift under \mathcal{H}_{L} . We will see in Section 7.2 that for this event, we could not find any evidence for a type-II (i.e., $n = 1/2$) lensed signal, and therefore we will drop the summation over n in the marginal likelihood. Similarly, the marginal likelihood under \mathcal{H}_{NL} is given by

$$p(d_{\text{GW}}|\mathcal{H}_{\text{NL}}) \propto \int dz_s p_{\text{pop}}(z_s|\mathcal{H}_{\text{NL}}) \left[\int dm_1^{\text{src}} dm_2^{\text{src}} \right. \\ \left. p(d_{\text{GW}}|m_{1,2}^{\text{det}} = (1 + z_s)m_{1,2}^{\text{src}}, D_{\text{L}} = D_{\text{L}}^{\text{src}}) p_{\text{pop}}(m_1^{\text{src}}, m_2^{\text{src}}) \right], \quad (13)$$

and again the term enclosed by the square brackets is the marginal likelihood $\mathcal{L}_{\mathcal{H}_{\text{NL}}}(z_s)$ as a function of the source redshift under this hypothesis.

Using the hanabi.hierarchical code (Lo & Magana Hernandez 2023) and assuming $p(\mu) \propto \mu^{-3}$ (Schneider et al. 1992)⁴, we compute the Bayes factor for GW230529 to be $\approx 1 : 58$ disfavoring the lensed hypothesis. This is consistent with intuition from the overall lensing rates and from the illustrative Figs. 3 and 4: the gain in consistency with population expectations from a lighter primary is not sufficient to overcome the penalty from needing the GW signal to be lensed with a sufficient magnification. Combined with the prior odds for the lensed versus the not-lensed hypothesis, related to the relative rate of lensed events estimated as $\lesssim 2 \times 10^{-3}$ in Section 4.1, statistically speaking GW230529 is unlikely to be magnified significantly.

⁴ Selection effects are accounted for in the normalization of the marginal likelihoods. Therefore, the prior for the magnification $p(\mu)$ to be used in the Bayes factor calculation should be the one *without* the selection effects, which is different from the expected distribution, e.g., in Fig. 2.

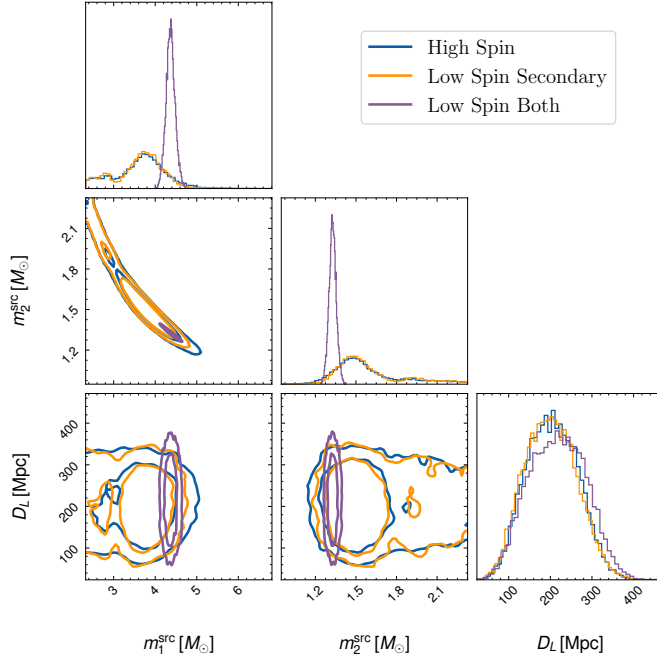


Figure 5. Posterior distributions for the source-frame component masses and the luminosity distance for analyses from [LVK \(2024a\)](#) done under the unlensed hypothesis, with the IMRPhenomXPHM waveform and different spin priors. The unconstrained (“high spin”) prior and the one with a constraint only on the secondary object’s spin (“low spin secondary”) give roughly the same results. The “low spin both” prior leads to a preference for more asymmetric masses.

6 PROPERTIES OF GW230529 UNDER THE LENSING HYPOTHESIS AND CONSISTENCY WITH OBSERVATIONS

6.1 A lensed binary with a neutron star as the primary?

To further investigate whether GW230529 could be a lensed BNS, we can correct for the potential lensing effect, *i.e.* find the source parameters assuming lensing, and see whether this gives a plausible system. To do so, we assume the primary to be a neutron star with a certain mass and see what would be the mass of the secondary, the source redshift, and the magnification. We can then verify whether these properties correspond to those expected in a lensed BNS system or to something more exotic or even non-physical.

We use three sets of results from [LVK \(2024a\)](#), all with the IMRPhenomXPHM waveform ([Pratten et al. 2021](#)) but with different priors:

- (i) one with sub-extremal spin amplitudes of the two components, $\chi_{1,2} \leq 0.99$, called “high spin”,
- (ii) one where the spin amplitude of the secondary is limited to 0.05, $\chi_2 \leq 0.05$, called “low spin secondary”,
- (iii) one where both spin amplitudes are limited below 0.05, $\chi_{1,2} \leq 0.05$, called “low spin both”.

In Fig. 5, we show the posterior distributions for the component masses and luminosity distance inferred under the unlensed hypothesis, with masses converted from the detector frame to the source frame using equation (5). The “low spin both” prior leads to preferring more asymmetric masses, while the two other results are broader,

with a preference for more symmetric masses, and similar to each other.

Under the hypothesis that GW230529 is lensed and the primary is a neutron star, we can instead use the neutron star mass distribution to pick a maximum source mass m_1^{src} , corresponding to the least degree of lensing required under that hypothesis. Now we can use equation (4) to compute the source redshift from the measured detector-frame primary mass. We can also find the source-frame mass for the secondary from the measured detector-frame value, using the same redshift with the same equation. Additionally, with equation (2) we can compute the magnification the event would have undergone for its masses to resemble those inferred for GW230529 under the unlensed hypothesis. Finally, assuming some EoS, it is then also possible to solve the Tolman-Oppenheimer-Volkoff equation and find the tidal deformabilities for the two components. Here, we use the maximum probability EoS from [Huth et al. \(2022\)](#). Note that we use this regardless of the spin amplitudes considered for the event.

Using this procedure, we investigate what kind of system could lead to observables similar to those of GW230529, under several choices for m_1^{src} : first, we pick the median, the lower and the upper quantiles at 90% confidence for the maximum mass of a neutron star from [LVK \(2023b\)](#), $1.99^{+0.29}_{-0.23} M_\odot$. To be conservative, we also include the possibility of the highest neutron star mass being $2.5 M_\odot$ ([Rocha et al. 2024; Fan et al. 2024](#)).

Results for the agnostic “high spin” prior and the four masses are shown in Fig. 6. We find significant support for the secondary being a sub-solar mass object, which would be considered exotic ([LVK 2023c](#)). Assuming the object is still made of nuclear matter, this leads to large tidal deformabilities. One could expect these to be measurable, which we will check further in the next two subsections. Additionally, when looking at the expected lensing parameters, we find the biggest support for relatively large magnifications, with a significant weight above $\mu = 10^3$, except for $m_1^{\text{src}} = 2.5 M_\odot$, where only $\sim 10\%$ of the samples are above this limit. This is still compatible with our expectations from population models but pushing into the less likely regime—see Fig. 2. The source redshift would still be relatively low, corresponding to low optical depth ([Oguri 2019](#)), *i.e.* a low lensing probability. In the end, only a limited fraction of the samples could lead to a viable lens-source system not requiring measurable tidal deformabilities or an exotic low-mass secondary object.

The “low spin secondary” prior leads to the same conclusions, though results are significantly different for the “low spin both” prior, as shown in Fig. 7. For simplicity, we now show only the highest and lowest primary mass considered before. With the “low spin both” prior, we always obtain a sub-solar mass secondary and extremely high tidal deformabilities. The magnifications would again be at the higher end of the distribution from our simulations, with higher support above $\mu = 10^3$, and also above 10^4 for $m_1^{\text{src}} = 1.76 M_\odot$. Source redshifts still stay below 2, matching the cut-off assumed in Section 4.2. Overall, imposing low spin constraints on both objects—as, in principle, expected for a BNS—leads to the most exotic results least compatible with an actual lensed BNS.

We summarize the probability for the lightest object to be sub-solar in the various cases in Table 3. For the “low spin both” prior, the secondary mass is always below $1 M_\odot$. If we assume the mass for a neutron star can be as low as $0.8 M_\odot$, the probability for the lightest object to be lower than this limit is 100%, except for the highest m_1^{src} considered, where it becomes 86.8%. So, if GW230529 was lensed and its spin amplitudes constrained below 0.05, then it would be nearly certain for the secondary to be a sub-solar mass object. Such an object would be astrophysically unexpected and either have

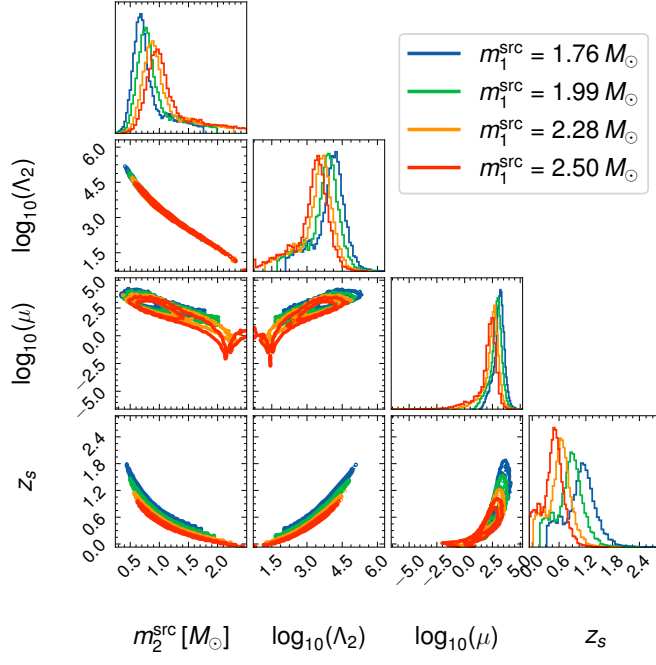


Figure 6. Posterior distributions under the lensed hypothesis for the inferred source-frame mass of the secondary object, its corresponding tidal deformability, as well as the magnification and source redshift. All results are obtained using the “high spin” prior, but we assume different primary masses. There is a non-negligible support for values in extreme regions (e.g. sub-solar mass, very high deformability) not matching the expectations for a lensed BNS or inconsistent with the GW230529 observation.

| \$m_1^{\text{src}} (M_\odot)\$ | High spin | Low spin secondary | Low spin both |
|--------------------------------|---------------|--------------------|---------------|
| 1.76 | 67.9% (50.8%) | 67.4% (51.1%) | 100% (100%) |
| 1.99 | 60.2% (34.2%) | 60.8% (33.8%) | 100% (100%) |
| 2.28 | 46.5% (16.3%) | 46.8% (14.5%) | 100% (99.9%) |
| 2.5 | 33.3% (8.5%) | 32.7% (6.7%) | 100% (86.8%) |

Table 3. Probability for the secondary of a lensed GW230529 to be lighter than $1 M_\odot$ (“sub-solar” objects) or (in parentheses) $0.8 M_\odot$ as a more conservative limit for the lightest neutron stars, for different prior choices from LVK (2024a). The “low spin both” prior leads to a quasi-certainty for the secondary to be sub-solar. For the other priors, this probability decreases as we allow higher masses for the primary, but always stays substantial.

very high tidal deformability or need to be a primordial black hole or a beyond standard model physics object. Therefore, what initially appears to be the most natural version of the BNS lensing scenario is unlikely to be consistent with an actual BNS and instead requires the addition of another low-probability phenomenon.

For the other spin priors, the probability for the secondary to be sub-solar is lower, but still substantial. While the system becomes less exotic in terms of masses, it would still require relatively high magnifications, and potentially large tidal deformabilities on the secondary (if it is not a black hole) to be compatible with the lensing hypothesis. Moreover, this corresponds to the case where the spins do not match our expectations for BNSs. So, should the event be lensed, it would still correspond to an astrophysically unexpected system.

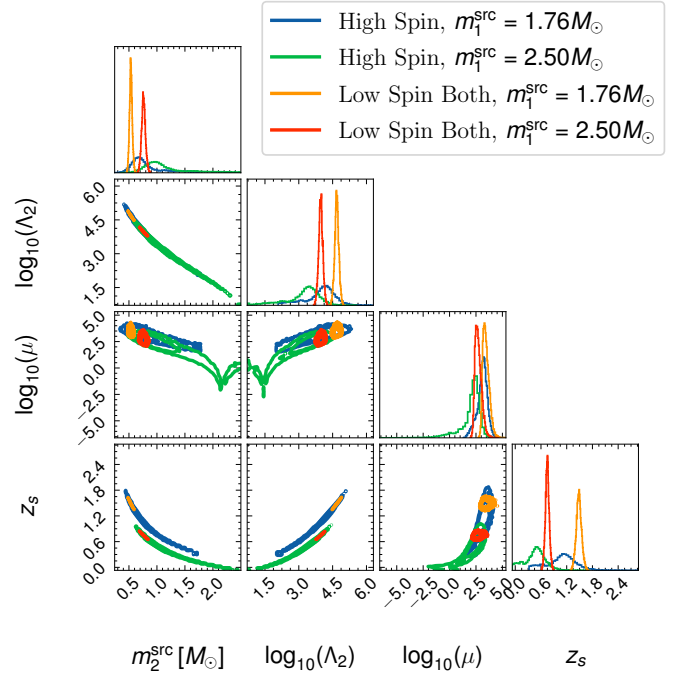


Figure 7. Posterior distributions under the lensed hypothesis for the “high spin” and “low spin both” priors, for the highest and lowest primary source mass considered before. The “low spin both” prior, designed to match expectations for BNSs, leads to more exotic results since the secondary would certainly be sub-solar, and the magnification much larger than expected.

6.2 Expected tidal deformabilities under the lensing hypothesis

As explained in Pang et al. (2020), if an event is lensed, there would be a discrepancy between the measured tidal deformability and the one expected from the source-frame masses found when undoing the lensing effects. Therefore, we now consider the tidal deformabilities measured in LVK (2024a) from the runs with the IMRPhenomPv2_NRTidalv2 waveform (Dietrich et al. 2019) and with two different priors: one with a low-spin constraint on the secondary, and one with a low-spin constraint on both objects. We compare these measurements against the deformabilities we would expect from the masses inferred under the lensing hypothesis.

After correcting for lensing as above, we again calculate the tidal deformabilities for the two objects by using the maximum probability EoS from Huth et al. (2022), and use equation (7) to find the distribution for $\tilde{\Lambda}$. This parameter is the best measured combination of tidal deformabilities since it appears at the lowest PN order in the waveform (Hinderer et al. 2010).

The left panel in Fig. 8 shows the $\tilde{\Lambda}$ distributions found for the “low spin secondary” prior with the different m_1^{src} choices as before, compared with the posterior found in the original analysis. The right panel shows the same for the “low spin both” prior. In the first case, the distributions found by correcting for the lensing effects are broad and span relatively low values, due to the higher masses expected for the secondary in this case. For the highest m_1^{src} choices, $\tilde{\Lambda}$ would be the lowest, which would likely lead to measurements that cannot exclude zero deformability. For $m_1^{\text{src}} < 2 M_\odot$, the range of possible values increases and part of the posterior would lead to measurable tidal deformabilities, contrary to what is seen. Still, in all cases, there is support for tidal deformability values compatible with the measured posteriors and with zero.

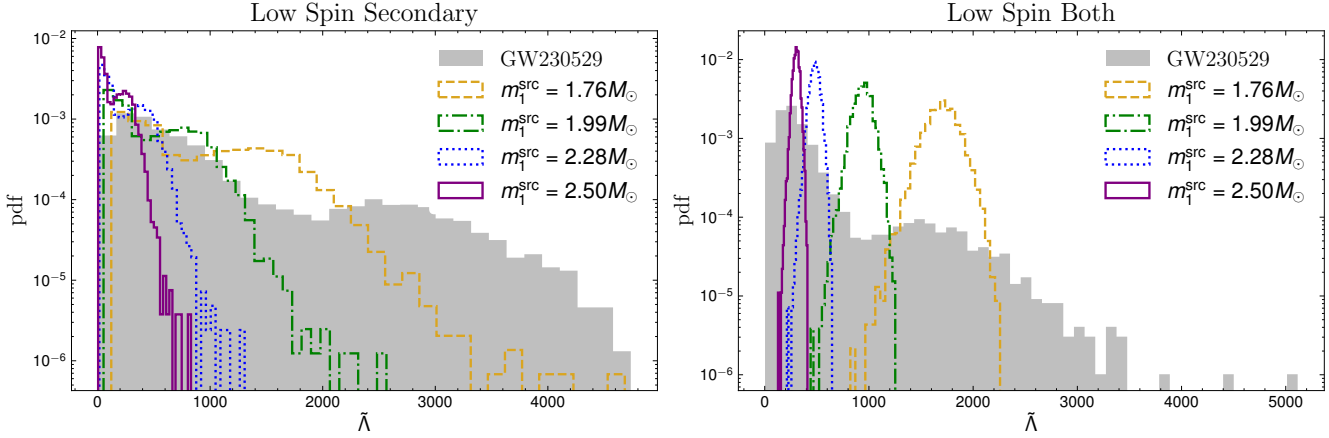


Figure 8. Comparison between the tidal deformability distributions expected for systems with GW230529’s masses after correcting for lensing and the measured ones. The left panel shows the results for the low-spin constraint on the secondary, while the right panel shows the results for the double low-spin constraint. The distributions are overlaid with the measured $\tilde{\Lambda}$ values measured for each spin priors used when analyzing the event with IMRPhenomPv2_NRTidalv2.

For the “low spin both” prior, shown in the right panel of Fig. 8, the distributions are more concentrated towards higher values, so that for $m_1^{src} < 2 M_\odot$ they begin to fall mostly in the lower density regions of the measurements. Therefore, should we have such tidal deformabilities, the highest mass cases would probably lead to a small enough $\tilde{\Lambda}$ to be unmeasurable. On the other hand, for the lowest m_1^{src} considered, most of the corresponding tidal deformabilities are high enough to be measurable and would lead to posteriors not compatible with zero, contrary to the observations from the GW230529 analyses.

6.3 Injection Studies

Going further, we can study with simulated signals if the high tidal deformability that a lensed low-mass secondary would present should have been observable in GW230529.

In Section 6.1 we have seen that, when correcting for the lensing effects, the secondary object tends to have low masses. Another implication is that $\tilde{\Lambda}$ is likely to be high for mergers containing such objects, since lower neutron star masses lead to higher tidal deformabilities. In a more general simulation study, Golomb et al. (2024) found that if both components are neutron stars and at least one is sub-solar, this should be clearly measurable. So, should the tidal deformability be measurable while the inferred source-frame component masses are relatively high, it would hint towards a possible lensed detection with overestimated masses (Pang et al. 2020).

We now take the maximum likelihood parameters from the results derived in Section 6.2 when accounting for lensing for the IMRPhenomPv2_NRTidalv2 waveform and inject them into Gaussian noise generated from the power spectral density for LIGO Livingston when GW230529 was observed (LVK 2024c). Then, we analyze them using the relative binning code from Narola et al. (2023) and verify whether the recovered tidal posteriors are more informative than those obtained on the real data. Both injection and recovery are done with the TaylorF2 waveform (Mishra et al. 2016) to avoid issues due to tapering faced with more complete models (Wouters et al. 2024). Moreover, BNS signals are dominated by the inspiral phase, where this waveform model matches well with other waveform models, such as those from the Phenom family. For reference, we also do the same analysis for an injection with zero tidal deformability.

The $\tilde{\Lambda}$ posteriors for the various injections are shown in Fig. 9. The left panel shows results based on the “low spin secondary” prior,

and the right panel for the “low spin both” prior. Since the tidal deformabilities of both components are larger for smaller m_1^{src} , the posteriors become more informative as we go down in m_1^{src} . From our injections, it seems like a posterior mostly consistent with zero is possible only if the primary is a black hole or a heavy neutron star with $m_1^{src} > 2.3 M_\odot$. On the contrary, the actual GW230529 posteriors for $\tilde{\Lambda}$ peak close to zero and are broadly compatible with this value, meaning they are not compatible with lower masses and more magnified events. Moreover, when doing the injections without tidal deformabilities, the recovered posteriors are consistent with zero and much closer to those for GW230529.

We note here that our injections were done only for the maximum likelihood values and a single EoS. More in-depth studies covering the entire posterior support and various EoSs would help increase our confidence in the conclusions from a non-measurable $\tilde{\Lambda}$ parameter. Still, our experiments indicate that the source is unlikely to have large tidal deformabilities and is closely consistent with the standard interpretation of an unlensed binary composed of a black hole and a neutron star, where one could also not measure $\tilde{\Lambda}$.

7 EXTRA CHECKS FOR LENSING FEATURES

Beyond considerations of population consistency and the observability of tidal deformations under the lensing scenario, it is also worth checking for direct signatures of lensing in the data of GW230529 and around it, using some of the methods previously developed for LVK lensing searches (LVC 2021; LVK 2024b).

7.1 Multiple Images

If a GW is strongly lensed, then we expect to be able to detect additional lensed GW images at different arrival times, which could range from minutes to years, depending on the mass and characteristics of the lens. In particular, we expect a highly magnified GW to have lensed counterparts with even shorter time delays, of the order of seconds to days (for example, see Smith et al. (2023) in the context of lensed BNS systems), and even overlapping with each other (Lo et al. 2024).

Regardless of the prior expectations on strong lensing discussed in the previous sections, it is still useful to try and search for potential

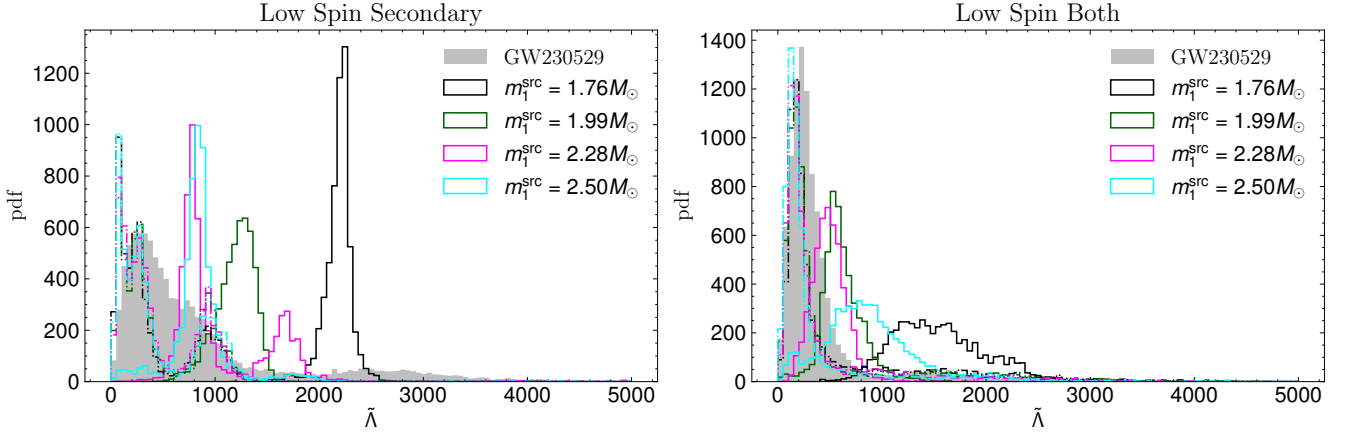


Figure 9. Posteriors for the $\tilde{\Lambda}$ parameter for maximum likelihood injections of the lensing-corrected parameters (solid lines), injections with zero tidal deformability for the secondary object (dot-dashed lines), and those from the parameter estimation runs for GW230529 with the same spin priors. The left panel shows the results for the “low spin” prior only on the secondary component, while the right panel shows the results for a “low spin both” prior. For both cases, the posterior when fixing $m_1^{\text{src}} = 2.5 M_{\odot}$ is still compatible with zero, although peaked away from that value. This compatibility with zero becomes much weaker if for lower $m_1^{\text{src}} = 2.28 M_{\odot}$, and $\tilde{\Lambda} = 0$ is excluded for the other assumed values. Meanwhile, for both priors the actual GW230529 posterior has support for zero, indicating that a lensed system with a primary of more conventional neutron star mass should have led to a different observation.

lensed GW counterparts of GW230529 in the data. Given that only 4096 seconds of data, centered around the time of the event, have been released for now, it is very challenging to perform the usual sub-threshold targeted searches (e.g., McIsaac et al. 2020; Li et al. 2023b,a). These would require a longer observation time to accumulate background triggers (due to noise) for proper assignment of statistical significance, such as a false-alarm rate, to triggers found by those searches.

Here, we opt to instead simply matched-filter the limited public data against a single template, as a *preliminary analysis*. Fig. 10 shows the SNR time series, computed using the PyCBC package⁵, when filtering the LIGO Livingston data against the maximum-likelihood waveform found by the parameter estimation analysis from LVK (2024a) using the IMRPhenomXPHM waveform model (Pratten et al. 2021). We have also used GstLAL to compute the SNR time series, and the result is consistent with the one shown here. The peak at time $t = 0$ s corresponds to GW230529.

There is a secondary peak, with a matched-filter SNR of ≈ 9 at $t \approx -1500$ s. This does not correspond to a genuine astrophysical signal since the corresponding trigger fails the signal consistency test in Allen (2005), with a reduced chi-square $\chi^2_r \gg 1$. Therefore, it is extremely inconsistent with a genuine GW and is likely due to non-Gaussian noise fluctuations (*i.e.* instrumental glitches). After discarding this spurious peak in the SNR time series at time $t \approx -1500$ s, there are no more obvious peaks (say, above a matched-filter SNR $\rho_{\text{L1}} > 8$) other than GW230529 itself.

We would like to stress again that this simplified analysis is *not* how a full search should be done, due to the absence of a statistically robust background estimation. The final verdict regarding any possible lensed counterparts of GW230529 would have to wait for the release and analysis of the complete O4a data. For now, preliminarily, we can say that we did not find any obvious GW signal with a similar waveform to GW230529 within the 4096 s of public data, with a relative magnification $\mu_{\text{rel}} \gtrsim (8/11.4)^2 \approx 1/2$ with respect to the known event.

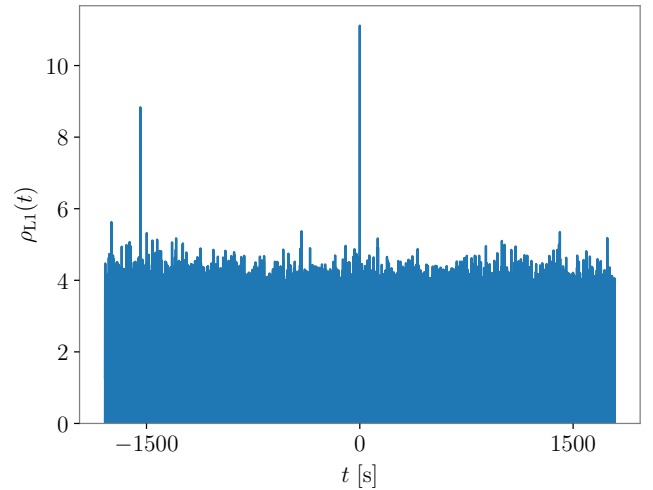


Figure 10. The SNR time series when filtering the 4096 s of LIGO Livingston data around GW230529 against the maximum-likelihood waveform found by the parameter estimation analysis from LVK (2024a) using the IMRPhenomXPHM waveform model. The peak at time $t = 0$ s corresponds to GW230529. The secondary peak at $t \approx -1500$ s, fails the signal consistency test in Allen (2005) and hence is inconsistent with a genuine GW signal.

7.2 Signals with Negative Parity

In order to tell a type-II (negative parity) signal and an unlensed signal apart, one will need to observe higher multipoles beyond the dominant quadrupolar GW emission from the data (Ezquiaga et al. 2021; Wang et al. 2021; Janquart et al. 2021b; Vijaykumar et al. 2023). Unfortunately, GW230529 is not particularly loud, and therefore we do not expect to be able to do so a-priori. Still, we went ahead and computed explicitly the Bayes factor $\mathcal{B}_{\text{unlensed}}^{\text{type II}}$ as the ratio of the evidence from a Bayesian parameter estimation using type-II and normal unlensed GW signal waveforms, respectively, as an indicator of the presence of imprints of a type-II signal in the

⁵ Not to be confused with the full PyCBC pipeline that uses the same codebase. Here we did not run the full search pipeline.

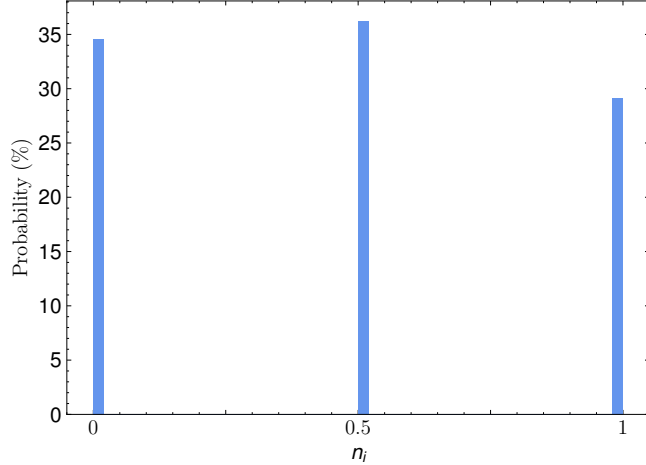


Figure 11. Posterior results from the GOLUM analysis for different image types. The posterior is inconclusive, showing no preference for any hypothesis, and thus we cannot tell whether GW230529 is a lensed type-II GW signal or not.

data. All analyses presented in this section were performed using the IMRPhenomXPHM waveform model (Pratten et al. 2021).

As expected, the log Bayes factor was found to be $\log_{10} \mathcal{B}_{\text{unlensed}}^{\text{type II}} = 0.04 \pm 0.10$ with the `hanabi.inference` code (Lo & Magana Hernandez 2023), which is smaller than its uncertainty coming from the nested sampling algorithm (Skilling 2006; Speagle 2020) when performing the Bayesian parameter estimation analyses. Therefore, we cannot tell whether GW230529 is a lensed type-II GW signal or not.

A similar analysis was performed using GOLUM (Janquart et al. 2021a, 2023a) to compute the probabilities comparing the hypotheses of a lensed type-II signal against lensed type-I or type-III signals, which allows for comparing the signal under all lensing image type hypotheses. The resulting posteriors for the Morse factor are shown in Fig. 11. The results are consistent with the type-II vs. unlensed analysis, yielding a very inconclusive posterior with equal support for any hypothesis. The resulting probabilities are $\ln(p(\text{IIvs.I})) = 0.05$ and $\ln(p(\text{IIvs.III})) = 0.22$. This leads to the same conclusion that we cannot tell whether GW230529 is a lensed type-II GW signal or not.

7.3 Microlensing Investigation

To further investigate the possibility of GW230529 being a lensed signal, we have also examined the data for any frequency-dependent waveform deformations that could be signatures of microlensing. This examination was conducted using the GRAVELAMPS framework (Wright & Hendry 2021) for each of the BBH, NSBH, and BNS cases. These were represented by the IMRPhenomXPHM (Pratten et al. 2021), IMRPhenomNSBH (Thompson et al. 2020), and IMRPhenomPv2_NRTidalv2 (Dietrich et al. 2019) waveform approximants, respectively. For this initial investigation, the isolated point-mass microlensing model was used, mirroring the investigations conducted both more widely (LVK 2024b) and in specific lensing investigations of previous events (Janquart et al. 2023b).

None of these investigations yielded significant support for the microlensing hypothesis with $\log_{10} \mathcal{B}_{\text{U}}^{\text{PM}}$ values of -0.014 , 0.098 , and -0.019 respectively. These values are all within the expected error on these log Bayes factors from the nested sampling algorithm (Skilling 2006; Speagle 2020).

Examination of the lens parameter posteriors for each of these investigations revealed that in all three cases they reflect the priors, which is the expectation for unlensed events. Similarly, comparisons of the chirp mass, mass ratio, and luminosity distance posteriors—those parameters likely to be most affected by the presence of microlensing—between the unlensed and lensed investigations did not reveal any significant differences between the posteriors consistent with an unlensed event.

Therefore, we conclude there is no significant evidence that GW230529 displays any signatures of microlensing.

8 CONCLUSIONS

As already discussed in LVK (2024a), it is difficult to confirm the exact nature of the component objects of the source of the GW230529 signal, particularly of the heavier component that appears to be within the purported $3\text{--}5 M_{\odot}$ mass gap. In this work, we have performed various explorations into the gravitational lensing hypothesis that would have made intrinsically lighter objects appear heavier in the GW observation. Overall, we find the lensing scenario is unlikely, based on current astrophysical assumptions.

In particular, our simulation-based estimates of lensed detection rates show that the chances for lensed BNS signals at O4a sensitivity are very low, with relative rates between lensed and unlensed events of 2×10^{-3} at most, with some variation depending on the assumed merger rate density. Hence, we would require numerous GW230529-like events before there is a reasonable chance of one being a lensed BNS. Moreover, by computing the Bayes factor accounting for the latest population models, we find a relatively strong disfavoring of the lensing hypothesis. Additionally, we have studied what the lensing and intrinsic source parameters would be under the lensing scenario. Here we find the event would likely require high magnifications, sometimes beyond expectations, and have a substantial probability for the lighter component being a sub-solar mass object. Therefore, adding the lensing hypothesis to the scenario generally does not lead to a less exotic source system. We have also looked for additional lensing signatures such as the presence of a second image in the 4096 s of publicly released data, the possibility of GW230529 being a type-II signal, and the presence of microlensing. In all cases, we find no evidence for these lensing-specific features.

Based on these investigations, we conclude that GW230529 is unlikely a lensed BNS masquerading as a mass-gap NSBH merger.

ACKNOWLEDGEMENTS

We thank the members of the LIGO–Virgo–KAGRA lensing group for useful discussions.

This research has made use of data or software obtained from the Gravitational Wave Open Science Center (gwosc.org), a service of the LIGO Scientific Collaboration, the Virgo Collaboration, and KAGRA. This material is based upon work supported by NSF’s LIGO Laboratory which is a major facility fully funded by the National Science Foundation, as well as the Science and Technology Facilities Council (STFC) of the United Kingdom, the Max-Planck-Society (MPS), and the State of Niedersachsen/Germany for support of the construction of Advanced LIGO and construction and operation of the GEO600 detector. Additional support for Advanced LIGO was provided by the Australian Research Council. Virgo is funded, through the European Gravitational Observatory (EGO), by the French Centre National de Recherche Scientifique (CNRS), the Italian Istituto Nazionale di

Fisica Nucleare (INFN) and the Dutch Nikhef, with contributions by institutions from Belgium, Germany, Greece, Hungary, Ireland, Japan, Monaco, Poland, Portugal, Spain. KAGRA is supported by Ministry of Education, Culture, Sports, Science and Technology (MEXT), Japan Society for the Promotion of Science (JSPS) in Japan; National Research Foundation (NRF) and Ministry of Science and ICT (MSIT) in Korea; Academia Sinica (AS) and National Science and Technology Council (NSTC) in Taiwan. The authors are grateful for computational resources provided by the LIGO Laboratory and supported by National Science Foundation Grants PHY-0757058 and PHY-0823459.

RL: Collect acknowledgements from people.

D. Keitel, N. Singh and A. Heffernan were supported by the Universitat de les Illes Balears (UIB); the Spanish Agencia Estatal de Investigación grants CNS2022-135440, PID2022-138626NB-I00, RED2022-134204-E, RED2022-134411-T, funded by MI-CIU/AEI/10.13039/501100011033, the European Union NextGenerationEU/PRTR, and the ERDF/EU; and the Comunitat Autònoma de les Illes Balears through the Direcció General de Recerca, Innovació i Transformació Digital with funds from the Tourist Stay Tax Law (PDR2020/11 - ITS2017-006) as well as through the Conselleria d'Economia, Hisenda i Innovació with grant numbers SINCO2022/6719 (European Union NextGenerationEU/PRTR-C17.I1) and SINCO2022/18146 (co-financed by the European Union and FEDER Operational Program 2021-2027 of the Balearic Islands).

R. Lo, J. Chan and J. M. Ezquiaga were supported by the research grant no. VIL37766 and no. VIL53101 from Villum Fonden, the DNRF Chair program grant no. DNRF162 by the Danish National Research Foundation and the European Union's Horizon 2020 research and innovation programme under the Marie Skłodowska-Curie grant agreement No 101131233. J. M. Ezquiaga is also supported by the Marie Skłodowska-Curie grant agreement No. 847523 INTER-ACTIONS. The Tycho supercomputer hosted at the SCIENCE HPC center at the University of Copenhagen was used for supporting this work.

L. Uronen is supported by the Hong Kong PhD Fellowship Scheme (HKPFS) from the Hong Kong Research Grants Council (RGC). H. Phurailatpam and L. Uronen acknowledge support by grants from the RGC of Hong Kong (Project No. CUHK 14304622 and 14307923), the start-up grant from the Chinese University of Hong Kong, and the Direct Grant for Research from the Research Committee of The Chinese University of Hong Kong.

This paper has been assigned document number LIGO-P2400353.

REFERENCES

Aasi, J., et al. 2015, *Class. Quant. Grav.*, 32, 074001, doi: [10.1088/0264-9381/32/7/074001](https://doi.org/10.1088/0264-9381/32/7/074001)

Acernese, F., et al. 2015, *Class. Quant. Grav.*, 32, 024001, doi: [10.1088/0264-9381/32/2/024001](https://doi.org/10.1088/0264-9381/32/2/024001)

Adams, T., Buskulic, D., Germain, V., et al. 2016, *Class. Quant. Grav.*, 33, 175012, doi: [10.1088/0264-9381/33/17/175012](https://doi.org/10.1088/0264-9381/33/17/175012)

Agathos, M., Meidam, J., Del Pozzo, W., et al. 2015, *Phys. Rev. D*, 92, 023012, doi: [10.1103/PhysRevD.92.023012](https://doi.org/10.1103/PhysRevD.92.023012)

Ahumada, T., et al. 2024. <https://arxiv.org/abs/2405.12403>

Akutsu, T., Ando, M., Arai, K., et al. 2020, arXiv e-prints, arXiv:2005.05574. <https://arxiv.org/abs/2005.05574>

Allen, B. 2005, *Phys. Rev. D*, 71, 062001, doi: [10.1103/PhysRevD.71.062001](https://doi.org/10.1103/PhysRevD.71.062001)

Allen, B., Anderson, W. G., Brady, P. R., Brown, D. A., & Creighton, J. D. E. 2012, *Phys. Rev. D*, 85, 122006, doi: [10.1103/PhysRevD.85.122006](https://doi.org/10.1103/PhysRevD.85.122006)

Aso, Y., Michimura, Y., Somiya, K., et al. 2013, *Phys. Rev. D*, 88, 043007, doi: [10.1103/PhysRevD.88.043007](https://doi.org/10.1103/PhysRevD.88.043007)

Aubin, F., et al. 2021, *Class. Quant. Grav.*, 38, 095004, doi: [10.1088/1361-6382/abe913](https://doi.org/10.1088/1361-6382/abe913)

Bauswein, A., Janka, H. T., Hebeler, K., & Schwenk, A. 2012, *Phys. Rev. D*, 86, 063001, doi: [10.1103/PhysRevD.86.063001](https://doi.org/10.1103/PhysRevD.86.063001)

Bauswein, A., Stergioulas, N., & Janka, H. T. 2014, *Phys. Rev. D*, 90, 023002, doi: [10.1103/PhysRevD.90.023002](https://doi.org/10.1103/PhysRevD.90.023002)

Belczynski, K., et al. 2020, *Astron. Astrophys.*, 636, A104, doi: [10.1051/0004-6361/201936528](https://doi.org/10.1051/0004-6361/201936528)

Bernuzzi, S., Dietrich, T., & Nagar, A. 2015, *Phys. Rev. Lett.*, 115, 091101, doi: [10.1103/PhysRevLett.115.091101](https://doi.org/10.1103/PhysRevLett.115.091101)

Bianconi, M., Smith, G. P., Nicholl, M., et al. 2023, *Mon. Not. Roy. Astron. Soc.*, 521, 3421, doi: [10.1093/mnras/stad673](https://doi.org/10.1093/mnras/stad673)

Canevarolo, S., van Vorsteren, L., & Chisari, N. E. 2024. <https://arxiv.org/abs/2404.11480>

Cannon, K., Caudill, S., Chan, C., et al. 2021, *SoftwareX*, 14, 100680, doi: [10.1016/j.softx.2021.100680](https://doi.org/10.1016/j.softx.2021.100680)

Chandra, K., Gupta, I., Gamba, R., et al. 2024. <https://arxiv.org/abs/2405.03841>

Chattopadhyay, D., Al-Shammari, S., Antonini, F., et al. 2024. <https://arxiv.org/abs/2407.08719>

Cutler, C., & Flanagan, E. E. 1994, *Phys. Rev. D*, 49, 2658, doi: [10.1103/PhysRevD.49.2658](https://doi.org/10.1103/PhysRevD.49.2658)

Dai, L., & Venumadhab, T. 2017. <https://arxiv.org/abs/1702.04724>

Dai, L., Zackay, B., Venumadhab, T., Roulet, J., & Zaldarriaga, M. 2020, arXiv e-prints. <https://arxiv.org/abs/2007.12709>

Dal Canton, T., Nitz, A. H., Gadre, B., et al. 2021, *Astrophys. J.*, 923, 254, doi: [10.3847/1538-4357/ac2f9a](https://doi.org/10.3847/1538-4357/ac2f9a)

Damour, T., & Nagar, A. 2009, *Phys. Rev. D*, 80, 084035, doi: [10.1103/PhysRevD.80.084035](https://doi.org/10.1103/PhysRevD.80.084035)

Davies, G. S., Dent, T., Tápai, M., et al. 2020, *Phys. Rev. D*, 102, 022004, doi: [10.1103/PhysRevD.102.022004](https://doi.org/10.1103/PhysRevD.102.022004)

Deguchi, S., & Watson, W. D. 1986, *Phys. Rev. D*, 34, 1708, doi: [10.1103/PhysRevD.34.1708](https://doi.org/10.1103/PhysRevD.34.1708)

Diego, J. M., Broadhurst, T., & Smoot, G. 2021, *Phys. Rev. D*, 104, 103529, doi: [10.1103/PhysRevD.104.103529](https://doi.org/10.1103/PhysRevD.104.103529)

Dietrich, T., Samajdar, A., Khan, S., et al. 2019, *Phys. Rev. D*, 100, 044003, doi: [10.1103/PhysRevD.100.044003](https://doi.org/10.1103/PhysRevD.100.044003)

Essick, R. 2023, *Phys. Rev. D*, 108, 043011, doi: [10.1103/PhysRevD.108.043011](https://doi.org/10.1103/PhysRevD.108.043011)

Essick, R., & Landry, P. 2020, *Astrophys. J.*, 904, 80, doi: [10.3847/1538-4357/abbd3b](https://doi.org/10.3847/1538-4357/abbd3b)

Ewing, B., Huxford, R., Singh, D., et al. 2023, arXiv e-prints. <https://arxiv.org/abs/2305.05625>

Ezquiaga, J. M., Holz, D. E., Hu, W., Lagos, M., & Wald, R. M. 2021, *Phys. Rev. D*, 103, 064047, doi: [10.1103/PhysRevD.103.064047](https://doi.org/10.1103/PhysRevD.103.064047)

Ezquiaga, J. M., Hu, W., & Lo, R. K. L. 2023, *Phys. Rev. D*, 108, 103520, doi: [10.1103/PhysRevD.108.103520](https://doi.org/10.1103/PhysRevD.108.103520)

Fan, Y.-Z., Han, M.-Z., Jiang, J.-L., Shao, D.-S., & Tang, S.-P. 2024, *Phys. Rev. D*, 109, 043052, doi: [10.1103/PhysRevD.109.043052](https://doi.org/10.1103/PhysRevD.109.043052)

Farah, A. M., Fishbach, M., Essick, R., Holz, D. E., & Galauadegi, S. 2022, *Astrophys. J.*, 931, 108, doi: [10.3847/1538-4357/ac5f03](https://doi.org/10.3847/1538-4357/ac5f03)

Farr, W. M., Sravan, N., Cantrell, A., et al. 2011, *ApJ*, 741, 103, doi: [10.1088/0004-637X/741/2/103](https://doi.org/10.1088/0004-637X/741/2/103)

Fishbach, M., Essick, R., & Holz, D. E. 2020, *Astrophys. J. Lett.*, 899, L8, doi: [10.3847/2041-8213/aba7b6](https://doi.org/10.3847/2041-8213/aba7b6)

Flanagan, E. E., & Hinderer, T. 2008, *Phys. Rev. D*, 77, 021502, doi: [10.1103/PhysRevD.77.021502](https://doi.org/10.1103/PhysRevD.77.021502)

Gao, B., Tang, S.-P., Wang, H.-T., Yan, J., & Fan, Y.-Z. 2024, *Phys. Rev. D*, 110, 044022, doi: [10.1103/PhysRevD.110.044022](https://doi.org/10.1103/PhysRevD.110.044022)

Golomb, J., Legred, I., Chatzitoannou, K., Abac, A., & Dietrich, T. 2024, arXiv e-prints. <https://arxiv.org/abs/2403.07697>

Goyal, S., D., H., Kapadia, S. J., & Ajith, P. 2021, *Phys. Rev. D*, 104, 124057, doi: [10.1103/PhysRevD.104.124057](https://doi.org/10.1103/PhysRevD.104.124057)

Hanna, C., et al. 2020, *Phys. Rev. D*, 101, 022003, doi: [10.1103/PhysRevD.101.022003](https://doi.org/10.1103/PhysRevD.101.022003)

Hannuksela, O., Haris, K., Ng, K., et al. 2019, *Astrophys. J. Lett.*, 874, L2, doi: [10.3847/2041-8213/ab0c0f](https://doi.org/10.3847/2041-8213/ab0c0f)

Hannuksela, O. A., Collett, T. E., Çalışkan, M., & Li, T. G. F. 2020, *Mon. Not. R. Astron. Soc.*, 500, 3421, doi: [10.1093/mnras/staa200](https://doi.org/10.1093/mnras/staa200)

Roy. Astron. Soc., 498, 3395, doi: [10.1093/mnras/staa2577](https://doi.org/10.1093/mnras/staa2577)

Haris, K., Mehta, A. K., Kumar, S., Venumadhav, T., & Ajith, P. 2018. <https://arxiv.org/abs/1807.07062>

Harry, I., & Hinderer, T. 2018, *Class. Quant. Grav.*, 35, 145010, doi: [10.1088/1361-6382/aac7e3](https://doi.org/10.1088/1361-6382/aac7e3)

Hinderer, T., Lackey, B. D., Lang, R. N., & Read, J. S. 2010, *Phys. Rev. D*, 81, 123016, doi: [10.1103/PhysRevD.81.123016](https://doi.org/10.1103/PhysRevD.81.123016)

Huang, Q.-G., Yuan, C., Chen, Z.-C., & Liu, L. 2024, *JCAP*, 08, 030, doi: [10.1088/1475-7516/2024/08/030](https://doi.org/10.1088/1475-7516/2024/08/030)

Huth, S., et al. 2022, *Nature*, 606, 276, doi: [10.1038/s41586-022-04750-w](https://doi.org/10.1038/s41586-022-04750-w)

Ivezić, v., et al. 2019, *Astrophys. J.*, 873, 111, doi: [10.3847/1538-4357/ab042c](https://doi.org/10.3847/1538-4357/ab042c)

Janquart, J., Hannuksela, O. A., K., H., & Van Den Broeck, C. 2021a, *Mon. Not. Roy. Astron. Soc.*, 506, 5430, doi: [10.1093/mnras/stab1991](https://doi.org/10.1093/mnras/stab1991)

Janquart, J., Haris, K., Hannuksela, O. A., & Van Den Broeck, C. 2023a, *Mon. Not. Roy. Astron. Soc.*, 526, 3088, doi: [10.1093/mnras/stad2838](https://doi.org/10.1093/mnras/stad2838)

Janquart, J., Seo, E., Hannuksela, O. A., Li, T. G. F., & Broeck, C. V. D. 2021b, *Astrophys. J. Lett.*, 923, L1, doi: [10.3847/2041-8213/ac3bcf](https://doi.org/10.3847/2041-8213/ac3bcf)

Janquart, J., et al. 2023b, *Mon. Not. Roy. Astron. Soc.*, 526, 3832, doi: [10.1093/mnras/stad2909](https://doi.org/10.1093/mnras/stad2909)

Julié, F.-L., Pompili, L., & Buonanno, A. 2024. <https://arxiv.org/abs/2406.13654>

Koehn, H., Wouters, T., Rose, H., et al. 2024. <https://arxiv.org/abs/2407.07837>

Koopmans, L. V. E., Bolton, A., Treu, T., et al. 2009, *ApJ*, 703, L51, doi: [10.1088/0004-637X/703/1/L51](https://doi.org/10.1088/0004-637X/703/1/L51)

Laarakkers, W. G., & Poisson, E. 1999, *Astrophys. J.*, 512, 282, doi: [10.1086/306732](https://doi.org/10.1086/306732)

Li, A. K. Y., Chan, J. C. L., Fong, H., et al. 2023a. <https://arxiv.org/abs/2311.06416>

Li, A. K. Y., Lo, R. K. L., Sachdev, S., et al. 2023b, *Phys. Rev. D*, 107, 123014, doi: [10.1103/PhysRevD.107.123014](https://doi.org/10.1103/PhysRevD.107.123014)

Li, S.-S., Mao, S., Zhao, Y., & Lu, Y. 2018, *Mon. Not. Roy. Astron. Soc.*, 476, 2220, doi: [10.1093/mnras/sty411](https://doi.org/10.1093/mnras/sty411)

Liu, A., Wong, I. C. F., Leong, S. H. W., et al. 2023, *Mon. Not. Roy. Astron. Soc.*, 525, 4149, doi: [10.1093/mnras/stad1302](https://doi.org/10.1093/mnras/stad1302)

Liu, X., Magana Hernandez, I., & Creighton, J. 2021, *Astrophys. J.*, 908, 97, doi: [10.3847/1538-4357/abd7eb](https://doi.org/10.3847/1538-4357/abd7eb)

Lo, R. K. L., & Magana Hernandez, I. 2023, *Phys. Rev. D*, 107, 123015, doi: [10.1103/PhysRevD.107.123015](https://doi.org/10.1103/PhysRevD.107.123015)

Lo, R. K. L., Vujeva, L., Ezquiaga, J. M., & Chan, J. C. L. 2024, arXiv e-prints. <https://arxiv.org/abs/2407.17547>

LVC. 2018, *Phys. Rev. Lett.*, 121, 161101, doi: [10.1103/PhysRevLett.121.161101](https://doi.org/10.1103/PhysRevLett.121.161101)

—. 2021, *Astrophys. J.*, 923, 14, doi: [10.3847/1538-4357/ac23db](https://doi.org/10.3847/1538-4357/ac23db)

LVK. 2023a, *Phys. Rev. X*, 13, 041039, doi: [10.1103/PhysRevX.13.041039](https://doi.org/10.1103/PhysRevX.13.041039)

—. 2023b, *Phys. Rev. X*, 13, 011048, doi: [10.1103/PhysRevX.13.011048](https://doi.org/10.1103/PhysRevX.13.011048)

—. 2023c, *Mon. Not. Roy. Astron. Soc.*, 524, 5984, doi: [10.1093/mnras/stad588](https://doi.org/10.1093/mnras/stad588)

—. 2024a, *Astrophys. J. Lett.*, 970, L34, doi: [10.3847/2041-8213/ad5beb](https://doi.org/10.3847/2041-8213/ad5beb)

—. 2024b, *Astrophys. J.*, 970, 191, doi: [10.3847/1538-4357/ad3e83](https://doi.org/10.3847/1538-4357/ad3e83)

—. 2024c, Observation of Gravitational Waves from the Coalescence of a 2.5-4.5 Msun Compact Object and a Neutron Star — Data Release, Zenodo, doi: [10.5281/zenodo.10845779](https://doi.org/10.5281/zenodo.10845779)

Magare, S., Kapadia, S. J., More, A., et al. 2023, *Astrophys. J. Lett.*, 955, L31, doi: [10.3847/2041-8213/acf668](https://doi.org/10.3847/2041-8213/acf668)

Magare, S., More, A., & Choudary, S. 2024. <https://arxiv.org/abs/2403.02994>

Matas, A., et al. 2020, *Phys. Rev. D*, 102, 043023, doi: [10.1103/PhysRevD.102.043023](https://doi.org/10.1103/PhysRevD.102.043023)

McIsaac, C., Keitel, D., Collett, T., et al. 2020, *Phys. Rev. D*, 102, 084031, doi: [10.1103/PhysRevD.102.084031](https://doi.org/10.1103/PhysRevD.102.084031)

Messick, C., et al. 2017, *Phys. Rev. D*, 95, 042001, doi: [10.1103/PhysRevD.95.042001](https://doi.org/10.1103/PhysRevD.95.042001)

Mishra, A., Meena, A. K., More, A., Bose, S., & Bagla, J. S. 2021, *Mon. Not. Roy. Astron. Soc.*, 508, 4869, doi: [10.1093/mnras/stab2875](https://doi.org/10.1093/mnras/stab2875)

Mishra, C. K., Kela, A., Arun, K. G., & Faye, G. 2016, *Phys. Rev. D*, 93, 084054, doi: [10.1103/PhysRevD.93.084054](https://doi.org/10.1103/PhysRevD.93.084054)

Mukherjee, S., Broadhurst, T., Diego, J. M., Silk, J., & Smoot, G. F. 2021, *Mon. Not. Roy. Astron. Soc.*, 506, 3751, doi: [10.1093/mnras/stab1980](https://doi.org/10.1093/mnras/stab1980)

Nakamura, T. T. 1998, *Phys. Rev. Lett.*, 80, 1138, doi: [10.1103/PhysRevLett.80.1138](https://doi.org/10.1103/PhysRevLett.80.1138)

Narola, H., Janquart, J., Meijer, Q., Haris, K., & Van Den Broeck, C. 2023. <https://arxiv.org/abs/2308.12140>

Ng, K. K. Y., Wong, K. W. K., Broadhurst, T., & Li, T. G. F. 2018, *Physical Review D*, 97, 023012, doi: [10.1103/PhysRevD.97.023012](https://doi.org/10.1103/PhysRevD.97.023012)

Nitz, A. H., Dent, T., Dal Canton, T., Fairhurst, S., & Brown, D. A. 2017, *Astrophys. J.*, 849, 118, doi: [10.3847/1538-4357/aa8f50](https://doi.org/10.3847/1538-4357/aa8f50)

Oguri, M. 2018, *Mon. Not. Roy. Astron. Soc.*, 480, 3842, doi: [10.1093/mnras/sty2145](https://doi.org/10.1093/mnras/sty2145)

—. 2019, *Rept. Prog. Phys.*, 82, 126901, doi: [10.1088/1361-6633/ab4fc5](https://doi.org/10.1088/1361-6633/ab4fc5)

Ohanian, H. C. 1974, *International Journal of Theoretical Physics*, 9, 425, doi: [10.1007/BF01810927](https://doi.org/10.1007/BF01810927)

O'Shaughnessy, R., Kim, C., Kalogera, V., & Belczynski, K. 2008, *ApJ*, 672, 479, doi: [10.1086/523620](https://doi.org/10.1086/523620)

Özel, F., Psaltis, D., Narayan, R., & McClintock, J. E. 2010, *ApJ*, 725, 1918, doi: [10.1088/0004-637X/725/2/1918](https://doi.org/10.1088/0004-637X/725/2/1918)

Pang, P. T. H., Hannuksela, O. A., Dietrich, T., Pagano, G., & Harry, I. W. 2020, *Monthly Notices of the Royal Astronomical Society*, 495, 3740, doi: [10.1093/mnras/staa1430](https://doi.org/10.1093/mnras/staa1430)

Phurailatpam, H., More, A., Narola, H., et al. 2024. <https://arxiv.org/abs/2407.07526>

Poisson, E. 1998, *Phys. Rev. D*, 57, 5287, doi: [10.1103/PhysRevD.57.5287](https://doi.org/10.1103/PhysRevD.57.5287)

Poon, J. S. C., Rinaldi, S., Janquart, J., Narola, H., & Hannuksela, O. A. 2024. <https://arxiv.org/abs/2406.06463>

Pratten, G., et al. 2021, *Phys. Rev. D*, 103, 104056, doi: [10.1103/PhysRevD.103.104056](https://doi.org/10.1103/PhysRevD.103.104056)

Rocha, L. S., Horvath, J. E., de Sá, L. M., et al. 2024, *Universe*, 10, 3, doi: [10.3390/universe10010003](https://doi.org/10.3390/universe10010003)

Ronchini, S., et al. 2024. <https://arxiv.org/abs/2405.10752>

Sachdev, S., et al. 2019, arXiv e-prints. <https://arxiv.org/abs/1901.08580>

Samajdar, A., & Dietrich, T. 2019, *Phys. Rev. D*, 100, 024046, doi: [10.1103/PhysRevD.100.024046](https://doi.org/10.1103/PhysRevD.100.024046)

Sänger, E. M., et al. 2024. <https://arxiv.org/abs/2406.03568>

Schneider, P., Ehlers, J., & Falco, E. E. 1992, *Gravitational Lenses*, *Astronomy and Astrophysics Library* (Springer), doi: [10.1007/978-3-662-03758-4](https://doi.org/10.1007/978-3-662-03758-4)

Seo, E., Li, T. G. F., & Hendry, M. A. 2023. <https://arxiv.org/abs/2311.05543>

Shaik, F. H., Lange, J., Field, S. E., et al. 2020, *Phys. Rev. D*, 101, 124054, doi: [10.1103/PhysRevD.101.124054](https://doi.org/10.1103/PhysRevD.101.124054)

Skilling, J. 2006, *Bayesian Analysis*, 1, 833, doi: [10.1214/06-BA127](https://doi.org/10.1214/06-BA127)

Smith, G. P., Robertson, A., Mahler, G., et al. 2023, *Mon. Not. Roy. Astron. Soc.*, 520, 702, doi: [10.1093/mnras/stad140](https://doi.org/10.1093/mnras/stad140)

Somiya, K. 2012, *Class. Quant. Grav.*, 29, 124007, doi: [10.1088/0264-9381/29/12/124007](https://doi.org/10.1088/0264-9381/29/12/124007)

Speagle, J. S. 2020, *Mon. Not. Roy. Astron. Soc.*, 493, 3132, doi: [10.1093/mnras/staa278](https://doi.org/10.1093/mnras/staa278)

Suwa, Y., Yoshida, T., Shibata, M., Umeda, H., & Takahashi, K. 2018, *Mon. Not. Roy. Astron. Soc.*, 481, 3305, doi: [10.1093/mnras/sty2460](https://doi.org/10.1093/mnras/sty2460)

Takahashi, R., & Nakamura, T. 2003, *Astrophys. J.*, 595, 1039, doi: [10.1086/377430](https://doi.org/10.1086/377430)

Thompson, J. E., Fauchon-Jones, E., Khan, S., et al. 2020, *Phys. Rev. D*, 101, 124059, doi: [10.1103/PhysRevD.101.124059](https://doi.org/10.1103/PhysRevD.101.124059)

Tsang, K. W., Dietrich, T., & Van Den Broeck, C. 2019, *Phys. Rev. D*, 100, 044047, doi: [10.1103/PhysRevD.100.044047](https://doi.org/10.1103/PhysRevD.100.044047)

Tsukada, L., et al. 2023, *Phys. Rev. D*, 108, 043004, doi: [10.1103/PhysRevD.108.043004](https://doi.org/10.1103/PhysRevD.108.043004)

Usman, S. A., et al. 2016, *Class. Quant. Grav.*, 33, 215004, doi: [10.1088/0264-9381/33/21/215004](https://doi.org/10.1088/0264-9381/33/21/215004)

Vijaykumar, A., Mehta, A. K., & Ganguly, A. 2023, *Phys. Rev. D*, 108, 043036, doi: [10.1103/PhysRevD.108.043036](https://doi.org/10.1103/PhysRevD.108.043036)

Vitale, S., Lynch, R., Raymond, V., et al. 2017, *Phys. Rev. D*, 95, 064053,

doi: [10.1103/PhysRevD.95.064053](https://doi.org/10.1103/PhysRevD.95.064053)
 Wang, Y., Lo, R. K. L., Li, A. K. Y., & Chen, Y. 2021, Phys. Rev. D, 103, 104055, doi: [10.1103/PhysRevD.103.104055](https://doi.org/10.1103/PhysRevD.103.104055)
 Wang, Y., Stebbins, A., & Turner, E. L. 1996, Phys. Rev. Lett., 77, 2875, doi: [10.1103/PhysRevLett.77.2875](https://doi.org/10.1103/PhysRevLett.77.2875)
 Wempe, E., Koopmans, L. V. E., Wierda, A. R. A. C., Hannuksela, O. A., & Broeck, C. v. d. 2022. <https://arxiv.org/abs/2204.08732>
 Wierda, A. R. A. C., Wempe, E., Hannuksela, O. A., Koopmans, L. e. V. E., & Van Den Broeck, C. 2021, *Astrophys. J.*, 921, 154, doi: [10.3847/1538-4357/ac1bb4](https://doi.org/10.3847/1538-4357/ac1bb4)
 Wierda, A. R. A. C., Wempe, E., Hannuksela, O. A., Koopmans, L. V. E., & Van Den Broeck, C. 2021, *ApJ*, 921, 154, doi: [10.3847/1538-4357/ac1bb4](https://doi.org/10.3847/1538-4357/ac1bb4)
 Witt, H. J. 1990, *A&A*, 236, 311
 Wouters, T., Pang, P. T. H., Dietrich, T., & Van Den Broeck, C. 2024. <https://arxiv.org/abs/2404.11397>
 Wright, M., & Hendry, M. 2021, doi: [10.3847/1538-4357/ac7ec2](https://doi.org/10.3847/1538-4357/ac7ec2)
 Wright, M., Janquart, J., & Hendry, M. 2023, *Astrophys. J.*, 959, 70, doi: [10.3847/1538-4357/ad0891](https://doi.org/10.3847/1538-4357/ad0891)
 Wysocki, D., Lange, J., & O'Shaughnessy, R. 2019, Phys. Rev. D, 100, 043012, doi: [10.1103/PhysRevD.100.043012](https://doi.org/10.1103/PhysRevD.100.043012)
 Xu, F., Ezquiaga, J. M., & Holz, D. E. 2022, *Astrophys. J.*, 929, 9, doi: [10.3847/1538-4357/ac58f8](https://doi.org/10.3847/1538-4357/ac58f8)
 Ye, C. S., Kremer, K., Ransom, S. M., & Rasio, F. A. 2024. <https://arxiv.org/abs/2408.00076>
 Zhu, J.-P., Hu, R.-C., Kang, Y., et al. 2024. <https://arxiv.org/abs/2404.10596>